Design of Complex Wave Digital Filters using the Cross Adaptor

by

Sinisa Aleksandar Iliskovic

A Thesis Presented to the Faculty of Graduate Studies

in Partial Fulfillment of the Requirements for the Degree

Master of Science

The Department of Electrical and Computer Engineering

University of Manitoba

Winnipeg, Manitoba

January, 1998

THE UNIVERSITY OF MANITOBA

FACULTY OF GRADUATE STUDIES

*****

COPYRIGHT PERMISSION PAGE

DESIGN OF COMPLEX WAVE DIGITAL FILTERS USING THE CROSS ADAPTOR

BY

SINISA ALEKSANDAR ILISKOVIC

A Thesis/Practicum submitted to the Faculty of Graduate Studies of The University of Manitoba in partial fulfillment of the requirements of the degree of

MASTER OF SCIENCE

I hereby declare that I am the sole author of this thesis.

I authorize the University of Manitoba to lend this thesis to other institutions or individuals for the purpose of scholarly research.

Sinisa Aleksandar Iliskovic

I further authorize the University of Manitoba to reproduce this thesis by photocopying or by other means, in total or in part, at the request of other institutions or individuals for the purpose of scholarly research.

Sinisa Aleksandar Iliskovic

Abstract

The objective of this thesis is the design of complex wave digital filters (CWDFs) using the pipelineable unitary (PU) algorithm. The advantages of this method are the following:

1. The PU structure can be used for both normalized and denormalized representations of complex adaptors used in the realization of complex wave digital filters with a constraint that denormalized form can not be used without multipliers.
2. The PU algorithm allows for the decomposition of high order digital filters into a cascaded connection of simple PU building blocks.

The calculation of quantified coefficients is done using the Discrete Fourier Transform (DFT).

At the end, discussion and comparison of frequency responses for each type of realized CWDF has been provided with regard to one another and also with regard to the nominal frequency response of each of these CWDFs. It has been observed that filter design using PU algorithm with the two-port cross adaptor gave better results then two-port adaptor realization used in [4]. Also, this type of adaptor has only one coefficient to work with, namely β and β^* which differ only by the sign of the real part.

Acknowledgments

I would like to express my sincere gratitude to Professor Dr. G.O. Martens for his help during course of this research. Since I came to Canada five years ago, during my undergraduate and graduate studies, he was more than a Professor and Advisor to me, he was my friend.

Also special thanks to Dr. Gordon Scarth for his help in the field of Digital Filters.

This thesis is dedicated to my parents,

Nadežda and Aleksandar

TABLE OF CONTENTS

Chapter I

Introduction

A digital filter is best described as a digital system designed for the purpose of filtering discrete-time signals. Implementation of a digital filter can be done in software or with dedicated hardware or by combining software and hardware.

For example, the implementation of software digital filters can be done easily using simple programming on a digital signal processor (DSP) unit.

The advantages over analog filters are the following:

1. Small physical size.
2. High reliability.
3. Various kinds of noise do not affect the digital system which means that environmental signals would not affect systems performance [13].
4. Tolerance of components (temperature, aging, etc.) is vastly improved since component values do not change over time.
5. Very simple procedures are required if the characteristics of a digital filter such as a programmable filter or an adaptive filter [13] must be altered to suit new system or signal requirements.

The digital filter or digital system of interest for this thesis is a complex wave digital filter (CWDF) with the following properties:

1. Pipelineable [17]. This means that due to the decomposition of the digital filter into smaller substructures that are pipelined we can save computation time because one computation sequence can be started before the previous one has finished

(before the end of the loop). These pipelined substructures are referred to as pipelined cascades.

Pipelineability provides for tasks from multiple instances to be performed at the same time. This is not fully equivalent to parallelism because in parallel structures only tasks at the same instance are performed at the same time.

2. Complex.
3. Lossless.

Circuit derivation has been achieved with use of the PU algorithm [1] and modified for the WDF structures by Fettweis [2]. This algorithm is based on the iterative interchange of the h and f polynomials followed by the extraction of a QUARL, until a zeroth order section has been obtained. Calculations are done for a few different types of adaptors in both normalized and denormalized form using the Discrete Fourier Transform (DFT) for the polynomial calculations. The purpose of this thesis is to obtain the formulae for the Cross Adaptor [20] that can be used in the PU algorithm as a basic building block, and to show its advantages over a different type of adaptor [4] (the normalized parallel two-port adaptor), with respect to sensitivity, accuracy and ease of implementation.

V. Cheng [4] has used the normalized parallel two-port adaptor with unimodular multipliers to obtain PU blocks, whereas the structure shown in this thesis does not require any unimodular multipliers, except for the final section of the PU structure.

The Cross Adaptor was introduced by Schütte [20] who derived it from the parallel two-port adaptor using two additional unimodular multipliers.

The problem is obtaining efficient formulae easy to implement in the actual design and to check that all the properties of the filters and the cross adaptors themselves comply with the

theory and practice of wave digital filters.

In the Chapter 2 a theoretical overview of the necessary equations for this thesis is given. Also, the representation of two-port adaptors is discussed and given.

In the Chapter 3 formulae for the adaptors used in the design chapter are shown, diagrams of the corresponding adaptors and the frequency response equations as a result of the overall structure are given.

Also, a time-domain calculation is presented with a block diagram that makes the pipelineability of the derived structure obvious.

Equivalencies between normalized and denormalized cross adaptors are obtained and implementation steps for the PU algorithm are explained.

Chapter 4 deals with the design examples and results using different numbers of bits of precision for the calculated coefficients.

Chapter 5 contains the conclusions based on the previous chapters.

Chapter II

Theory Of Lossless Two-Port Networks

In this chapter, theoretical formulae necessary for the design of CWDFs are derived and discussed. Equations are derived from real lossless filters using voltage wave formulae by Fettweis [2].

2.1 Wave Variables and Scattering Coefficients

For the two-port network of Figure 2.1 we can define the following variables

$$A_i = V_i + R_i I_i \quad , \quad B_i = V_i - R_i I_i \qquad (2.1)$$

$i = 1, 2$ (for a two-port network)

where R_i is an arbitrary port reference, and A_i is an incident, and B_i a reflected voltage wave. V_i and I_i are the voltage and current defined for each port.

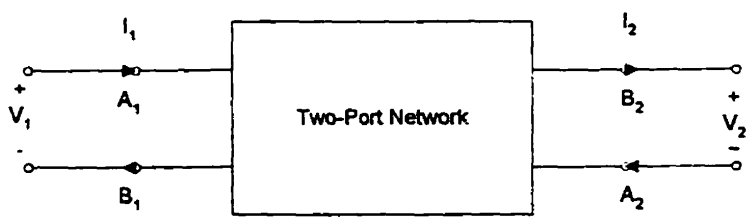

Figure 2.1 Two-Port Network

For a two-port(Fig. 2.1) the incident and reflected waves can be related by

$$\begin{pmatrix} B_1 \\ A_1 \end{pmatrix} = T \cdot \begin{pmatrix} A_2 \\ B_2 \end{pmatrix} \tag{2.2a}$$

where $T = \begin{pmatrix} T_{11} & T_{12} \\ T_{21} & T_{22} \end{pmatrix}$ is the transfer matrix. (2.2b)

Alternatively,

$$\begin{pmatrix} B_1 \\ B_2 \end{pmatrix} = S \cdot \begin{pmatrix} A_1 \\ A_2 \end{pmatrix} \qquad \text{where} \qquad S = \begin{pmatrix} S_{11} & S_{12} \\ S_{21} & S_{22} \end{pmatrix} \tag{2.3}$$

is the scattering matrix for a two-port network shown in Fig. 2.1.

For further work in this thesis it is important to show the relationship between the scattering matrix S and the transfer matrix T. Using Eq. (2.2) and Eq. (2.3) the following holds:

$$\begin{pmatrix} S_{11} & S_{12} \\ S_{21} & S_{22} \end{pmatrix} = \frac{1}{T_{22}} \cdot \begin{pmatrix} T_{12} & T_{11} \cdot T_{22} - T_{12} \cdot T_{21} \\ 1 & -T_{21} \end{pmatrix} \tag{2.4a}$$

and

$$\begin{pmatrix} T_{11} & T_{12} \\ T_{21} & T_{22} \end{pmatrix} = \frac{1}{S_{21}} \cdot \begin{pmatrix} S_{12} \cdot S_{21} - S_{11} \cdot S_{22} & S_{11} \\ -S_{22} & 1 \end{pmatrix} \tag{2.4b}$$

2.2 Two-Port Networks as Represented by Belevitch

In this thesis it is necessary to use the equations for the Scattering and Transfer matrices as given by Belevitch in the polynomial form. Instead of voltage waves incident and reflected power waves are used:

$$A_i = \frac{V_i + R_i \cdot I_i}{2 \cdot \sqrt{R_i}} \qquad B_i = \frac{V_i - R_i \cdot I_i}{2 \cdot \sqrt{R_i}} \qquad i = 1,2 \tag{2.5}$$

Belevitch has used three polynomials and a unimodular constant, namely, f, h, g and σ. Using these polynomials the matrices S and T can be expressed as:

$$S = \frac{1}{g} \cdot \begin{pmatrix} h & \sigma \cdot f_* \\ f & -\sigma \cdot h_* \end{pmatrix} \quad , \quad T = \frac{1}{f} \cdot \begin{pmatrix} \sigma \cdot g_* & h \\ \sigma \cdot h_* & g \end{pmatrix} \tag{2.6}$$

where the polynomials f, g, h and a unimodular constant σ must satisfy the following conditions:

1) $f = f(\psi)$, $g = g(\psi)$, $h = h(\psi)$ can be either complex or real polynomials and ψ is a complex frequency variable. The paraconjugate is defined through the complex conjugate with the following expression:

$$f_*(\psi) \equiv f^*(-\psi^*) \tag{2.7}$$

where the subscript asterisk represents the paraconjugate and the superscript asterisk represents the complex conjugate.

If we apply the Bilinear Transformation to ψ,

$$\psi = \frac{z-1}{z+1} = \frac{1-z^{-1}}{1+z^{-1}} \tag{2.8}$$

the following is obtained (see [22]):

$$f_*(z^{-1}) \equiv z^{-m} \cdot f^*(z^*) \quad , \quad g_*(z^{-1}) \equiv z^{-m} \cdot g^*(z^*) \quad , \quad h_*(z^{-1}) \equiv z^{-m} \cdot h^*(z^*) \tag{2.9}$$

m is the degree of the highest degree polynomial in the scattering matrix, S.

2) The three polynomials f, h and g must satisfy the losslessness condition given by the Feldtkeller equation

$$(|g|)^2 = (|h|)^2 + (|f|)^2 \quad , \quad \psi = j \cdot \phi \tag{2.10}$$

or by using analytic continuation:

$$gg_* = hh_* + ff_* \tag{2.11}$$

3) $g(\psi)$ is a Hurwitz polynomial with all its zeros in the left-hand ψ-plane, with $g(z^{-1})$ having all its zeros outside the unit circle in the z^{-1}-plane.

4) σ is a unimodular constant; i.e $|\sigma| = 1$ where $|\ |$ denotes the complex modulus.

5) For f/g which is the transmittance, and for h/g, which is the reflectance, the following must be satisfied:

$$\left|\frac{f}{g}\right| \leq 1 \quad , \quad \left|\frac{h}{g}\right| \leq 1 \tag{2.12}$$

for ψ on the imaginary axis or z^{-1} on the unit circle (this follows from Eq. 2.10). This is a condition that states that both of these functions, transmittance and reflectance are passive.

6) At transmission zeros with $Re\psi > 0$, it is necessary that

$$\left|\frac{h}{g}\right| < 1 \quad , \quad \left|\frac{h}{g}\right|_* > 1 \tag{2.13}$$

A given transfer function can be realized by identifying it either with f/g, called the transmittance, or with h/g, called the reflectance.

2.3 The Cascade Connection

The cascade connection of two lossless two-ports is considered. Because of the equations that are used for the PU algorithm in the next chapter, equations for the cascade connection of two lossless two-ports are derived using the scattering coefficients of the transfer matrices:

$$\begin{pmatrix} B_{1a} \\ A_{1a} \end{pmatrix} = \frac{1}{f_a} \cdot \begin{pmatrix} \sigma_a \cdot g_a & h_{a*} \\ \sigma_a \cdot h_a & g_{a*} \end{pmatrix} \cdot \begin{pmatrix} A_{2a} \\ B_{2a} \end{pmatrix} = T_a \cdot \begin{pmatrix} A_{2a} \\ B_{2a} \end{pmatrix} ,$$

$$\begin{pmatrix} B_{1b} \\ A_{1b} \end{pmatrix} = \frac{1}{f_b} \cdot \begin{pmatrix} \sigma_b \cdot g_{b*} & h_b \\ \sigma_b \cdot h_{b*} & g_b \end{pmatrix} \cdot \begin{pmatrix} A_{2b} \\ B_{2b} \end{pmatrix} = T_b \cdot \begin{pmatrix} A_{2b} \\ B_{2b} \end{pmatrix} \qquad (2.15a, b)$$

where a and b stand for two-port networks Na and Nb. From Figure 2.2. it is obvious that

$$V_{2a} = V_{1b} \quad , \quad I_{2a} = -I_{1b} \quad , \text{ and with } R_a = R_b \text{ [2]}, \quad A_{2a} = B_{1b} \text{ and } B_{2a} = A_{1b} \qquad (2.16)$$

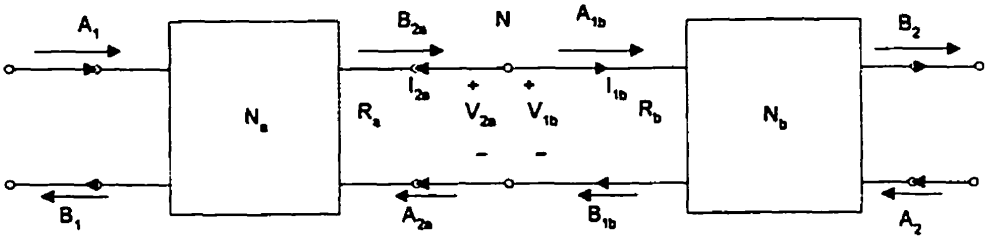

Figure 2.2 Cascade Connection of Two Two-Port Networks

From Eq. 2.15 and Eq. 2.16 we can calculate the transfer matrix for the overall two-port network of two cascaded two-ports by simply multiplying their transfer matrices to obtain

$$T = T_a \cdot T_b = \frac{1}{f} \cdot \begin{pmatrix} \sigma \cdot g & h \\ \sigma \cdot h & g \end{pmatrix} \qquad \text{where} \qquad (2.17)$$

$$\sigma = \sigma_a \cdot \sigma_b \quad , \quad f = f_a \cdot f_b \quad , \quad g = g_a \cdot g_b + \sigma_a \cdot h_a \cdot h_b \quad , \quad h = h_a \cdot g_b + \sigma_a \cdot g_a \cdot h_b \qquad (2.18)$$

For the PU algorithm it is important to determine equations for the T_b matrix if the T and T_a matrices are known. In other words, extracting T_a yields

$$T_b = (T_a)^{-1} \cdot T \qquad (2.19)$$

The first step is the extraction of a constant two-port T_a to obtain a factor z^{-1} from Eq. 2.19. The required factor is obtained by setting $h_b(0)=0$ which yields

$$-\frac{h}{g} \quad \text{evaluated at } z^{-1} = 0 \tag{2.20}$$

Because h/g is a reflectance hence bounded inside of the unit circle in the z^{-1}-plane this can be achieved. Also, remember that the network stays lossless because the extraction coefficient is also a lossless element.

$$T = \begin{pmatrix} T_{11} & T_{12} \\ T_{21} & T_{22} \end{pmatrix} \quad , \quad T^{-1} = \frac{1}{T_{11}\cdot T_{22} - T_{12}\cdot T_{21}} \cdot \begin{pmatrix} T_{22} & -T_{12} \\ -T_{21} & T_{11} \end{pmatrix} \tag{2.21}$$

Therefore from Eq. 2.17, Eq. 2.19 and Eq. 2.21

$$\begin{aligned} \sigma_b &= \sigma \\ f_b &= f\cdot\left(T_{11a}\cdot T_{22a} - T_{12a}\cdot T_{21a}\right) \\ g_b &= h\cdot\left(-T_{21a}\right) + g\cdot T_{11a} \\ h_b &= h\cdot T_{22a} + g\cdot\left(-T_{12a}\right) \end{aligned} \tag{2.22}$$

and the extraction factor is

$$-\left(\frac{h(0)}{g(0)}\right) = -\frac{T_{12a}}{T_{22a}}(0) \tag{2.23}$$

On the following pages specific values for the extraction factor are used based on the different types of constant two-ports that are going to be calculated. Also, the following sections and their PU equivalents must be introduced.

2.4 QUARL element and Unimodular Multiplier section

For further work in this thesis it is necessary to show the QUARL element and the Unimodular Multiplier in the form required for the PU structure.

A very important two-port is a quasi-reciprocal line, the QUARL[4]. The QUARL does not have the same delay in both directions, but the sum of the delays equals the delay of the corresponding Unit Element UE [4]. This is shown in Figure 2.3.

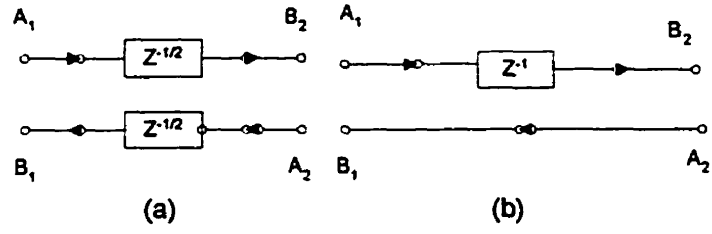

Figure 2.3 (a) Unit Element (b) QUARL element

The scattering and transfer matrices for a QUARL are given, respectively, by

$$S = \begin{pmatrix} 0 & 1 \\ z^{-1} & 0 \end{pmatrix} \quad , \quad T = \frac{1}{z^{-1}} \cdot \begin{pmatrix} z^{-1} & 0 \\ 0 & 1 \end{pmatrix} \tag{2.24a}$$

The unimodular multiplier section is a two-port element that can be used with a real two-port network to create a complex two-port network [21]. It is shown in Figure 2.4 .

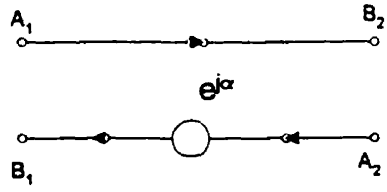

Figure 2.4 Unimodular Multiplier Section

The scattering and transfer matrices are also given for the unimodular multiplier section:

$$S = \begin{pmatrix} 0 & e^{j\cdot\alpha} \\ 1 & 0 \end{pmatrix} \quad , \quad T = \begin{pmatrix} e^{j\cdot\alpha} & 0 \\ 0 & 1 \end{pmatrix} \tag{2.24b}$$

2.5 Realization of Complex Wave Digital Filters

For the constant complex two-port network shown in Figure 2.5

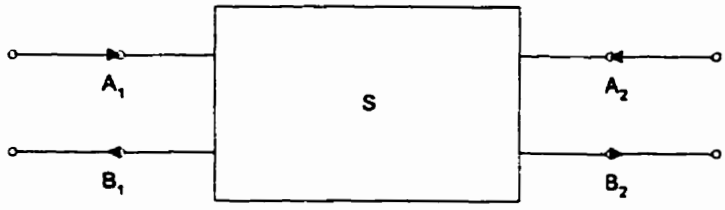

Figure 2.5 Complex Two-Port Network

with Scattering matrix from Eq 2.6

$$S = \frac{1}{g}\cdot\begin{pmatrix} h & \sigma\cdot f^{*} \\ f & -\sigma\cdot h^{*} \end{pmatrix}$$

where coefficients f, g, h and σ satisfy all conditions discussed earlier in this chapter, the following equations can be obtained:

For constant complex g, h, f and σ, they can be chosen as follows:

$$g = 1,\quad \sigma = e^{j\cdot\theta_1}\quad,\quad h = \beta = -r\cdot e^{j(\theta_1+\phi)} \tag{2.25}$$

where θ1 is included in the angle of β to obtain the desired forms in the following development.

Then $gg^{*} = hh^{*} + ff^{*}$ becomes

$$1 = (|h|)^2 + (|f|)^2 \quad \text{from which follows } |f| = \sqrt{1-(|\beta|)^2} = \sqrt{1-r^2} \tag{2.26}$$

and thus

$$f = \sqrt{1-r^2}\cdot e^{j\cdot\theta_2} \tag{2.27}$$

where θ_2 is arbitrary.

Then the scattering matrix S becomes

$$S = \begin{bmatrix} \beta & \sqrt{1-(|\beta|)^2}\cdot e^{-j\cdot(\theta_2-\theta_1)} \\ \sqrt{1-(|\beta|)^2}\cdot e^{j\cdot\theta_2} & -\beta^*\cdot e^{j\cdot\theta_1} \end{bmatrix} \tag{2.28a}$$

$$= \begin{bmatrix} -r\cdot e^{j\cdot(\phi+\theta_1)} & \sqrt{1-r^2}\cdot e^{-j\cdot(\theta_2-\theta_1)} \\ \sqrt{1-r^2}\cdot e^{j\cdot\theta_2} & r\cdot e^{-j\cdot\phi} \end{bmatrix} \tag{2.28b}$$

This is a very important equation for further work in this thesis. It gives us flexibility to determine different types of adaptors based on simply altering the angles ϕ, θ_1 and θ_2.

In the next few sections discussion and analysis of these different types of adaptors will be shown, based on Eq. 2.28b and different values of ϕ, θ_1 and θ_2. Depending on different choices for these angles, different adaptors are derived which will be used in the PU algorithm.

2.6 Complex Wave Digital Cross Adaptor--Normalized and Denormalized

For $\theta_1 = 0$ and $\theta_2 = 0$ we obtain

$$S = \begin{pmatrix} -r\cdot e^{j\cdot\phi} & \sqrt{1-r^2} \\ \sqrt{1-r^2} & r\cdot e^{-j\cdot\phi} \end{pmatrix} \tag{2.29}$$

Eq. 2.29 is the scattering matrix of the normalized complex wave digital cross adaptor [20].

Now if a diagonal similarity transformation [5] is used to scale (denormalize) the matrix S, where the scaling matrix D is:

$$D = \begin{pmatrix} 1 & 0 \\ 0 & \sqrt{1-r^2} \end{pmatrix} \quad , \quad D^{-1} = \begin{bmatrix} 1 & 0 \\ 0 & \dfrac{1}{\sqrt{1-r^2}} \end{bmatrix} \tag{2.30}$$

the following is obtained

$$D\cdot S\cdot D^{-1} = \begin{pmatrix} 1 & 0 \\ 0 & \sqrt{1-r^2} \end{pmatrix}\cdot\begin{pmatrix} -r\cdot e^{j\cdot\phi} & \sqrt{1-r^2} \\ \sqrt{1-r^2} & r\cdot e^{-j\cdot\phi} \end{pmatrix}\cdot\begin{bmatrix} 1 & 0 \\ 0 & \dfrac{1}{\sqrt{1-r^2}} \end{bmatrix} = \begin{pmatrix} -r\cdot e^{j\cdot\phi} & 1 \\ 1-r^2 & r\cdot e^{-j\cdot\phi} \end{pmatrix} \tag{2.31}$$

By introducing the substitution

$$\beta = -r\cdot e^{j\cdot\phi} \tag{2.32}$$

the new scattering matrix S is of the form

$$S = \begin{bmatrix} \beta & 1 \\ 1-(|\beta|)^2 & -\beta^* \end{bmatrix} = \begin{pmatrix} 0 & 1 \\ 1 & -\beta^* \end{pmatrix}\cdot\begin{pmatrix} 1 & 0 \\ \beta & 1 \end{pmatrix} \tag{2.33}$$

Eq. 2.33 represents the complex cross adaptor in the denormalized form. A symbolic representation of this adaptor is given in Figure 2.6. An important thing to note is that the two coefficients β and $-\beta^*$ are different only with regard to the sign of their real parts. This means that there is only one coefficient to quantize. A constraint to consider in this case is that these coefficients must have magnitude less than unity [5]. R_1 and R_2 are real [20].

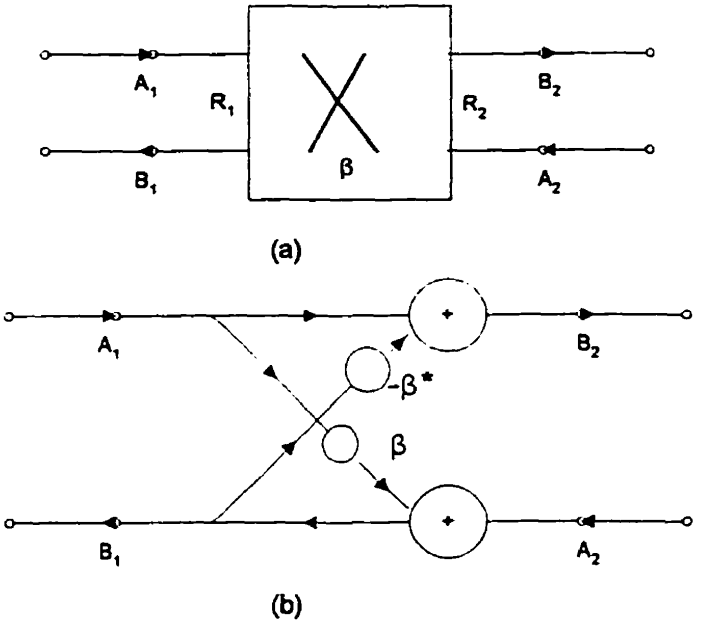

Figure 2.6 (a) Symbolic Representation of Complex Cross Adaptor,

(b) Signal-flow Diagram of Complex Cross Adaptor

The important thing is to see if this structure satisfies pseudolosslessness. Obviously it is not unitary because $S_* S \neq I$ where S_* is the paraconjugate-transpose of S and I is the identity matrix.

Choose:

$$G = \left(D^{-1}\right)^2$$

This is the condition for pseudolosslessness where G is diagonal matrix with $G_1 = 1$ and $G_2 = \dfrac{1}{1-(|\beta|)^2}$.

$$S^{*T}GS = \begin{bmatrix} \beta^* & 1-(|\beta|)^2 \\ 1 & -\beta \end{bmatrix} \cdot \begin{bmatrix} 1 & 0 \\ 0 & \dfrac{1}{1-(|\beta|)^2} \end{bmatrix} \cdot \begin{bmatrix} \beta & 1 \\ 1-(|\beta|)^2 & -\beta^* \end{bmatrix} = G \qquad (2.34)$$

Hence $G_2 > 0$, is equivalent to

$$(|\beta|)^2 < 1 \qquad (2.35)$$

The port references R_1 and R_2 are given by $R_1 = 1/G_1$ and $R_2 = 1/G_2$.

2.7 Complex Wave Digital Adaptor Represented in terms of a Real Wave Digital Adaptor

If $\theta_1 = -\phi$ and $\theta_2 = \theta_1$ in Eq. 2.28b, then

$$S = \begin{pmatrix} -r & \sqrt{1-r^2} \\ \sqrt{1-r^2}\cdot e^{-j\cdot\phi} & r\cdot e^{-j\cdot\phi} \end{pmatrix} = \begin{pmatrix} 1 & 0 \\ 0 & e^{-j\cdot\phi} \end{pmatrix} \cdot \begin{pmatrix} -r & \sqrt{1-r^2} \\ \sqrt{1-r^2} & r \end{pmatrix} \qquad (2.36)$$

The Eq. 2.36 is the matrix of a normalized complex wave adaptor. It is obvious that this matrix can be represented as a product of two matrices: a unimodular multiplier matrix and a normalized two-port parallel adaptor matrix.

$$S = \begin{pmatrix} 1 & 0 \\ 0 & e^{-j\cdot\phi} \end{pmatrix} \cdot \begin{pmatrix} -r & \sqrt{1-r^2} \\ \sqrt{1-r^2} & r \end{pmatrix} \tag{2.37}$$

Substituting r=cosθ and $\phi = 0$, the normalized real two-port adaptor scattering matrix is obtained:

$$S = \begin{pmatrix} -\cos\theta & \sin\theta \\ \sin\theta & \cos\theta \end{pmatrix} \tag{2.38}$$

Note: An ideal transformer in the analog domain is equivalent to a normalized digital parallel two-port adaptor. Both forms of the adaptor can be used for the purpose of the PU algorithm but since the objective is to keep the development as general as possible, general formula will be used. In this way it is easy to compare it with other types of CWDFs.

A symbolic representation for the digital equivalent of the ideal normalized transformer is shown in Figure 2.7 [4].

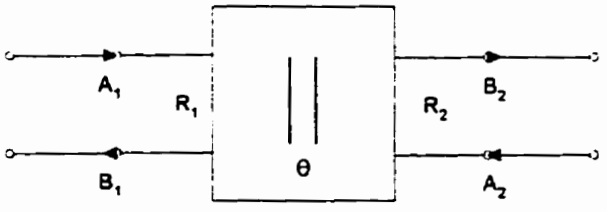

Figure 2.7 Normalized Parallel Two-Port Adaptor

Now, just as in the previous section a scaling factor is introduced:

$$D \cdot S \cdot D^{-1} = \begin{pmatrix} 1 & 0 \\ 0 & e^{-j\cdot\phi} \end{pmatrix} \cdot \begin{pmatrix} -r & 1+r \\ 1-r & r \end{pmatrix} \tag{2.39}$$

where

$$D = \begin{bmatrix} 1 & 0 \\ 0 & \dfrac{\sqrt{1-r^2}}{1+r} \end{bmatrix} \tag{2.40}$$

and S is given by Eq. 2.37.

The result of this scaling is a product of a unimodular multiplier matrix and the denormalized real parallel two-port adaptor as shown by the following equation:

$$S = \begin{pmatrix} 1 & 0 \\ 0 & e^{-j\cdot\phi} \end{pmatrix} \cdot \begin{pmatrix} -r & 1+r \\ 1-r & r \end{pmatrix} \tag{2.41}$$

where S is a denormalized scattering matrix.

If r is replaced with γ, the usual formula for the real two-port adaptor is obtained for the second matrix in Eq. 2.41. Figure 2.8 shows the real digital parallel two-port adaptor which is an equivalent of the denormalized ideal transformer.

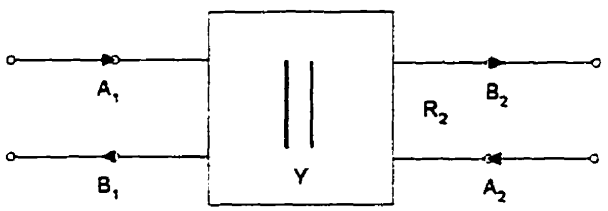

Figure 2.8 Real Parallel Two-Port Adaptor

The scattering matrix for the two-port adaptor is

$$S = \begin{pmatrix} -\gamma & 1+\gamma \\ 1-\gamma & \gamma \end{pmatrix} \tag{2.42}$$

In the next chapter the focus is on the PU algorithm and the application of the transfer matrices of the constant sections discussed above. Also, a process for obtaining the frequency response will be given together with a brief overview of the DFT that is used to calculate the adaptor coefficients. It is important to note that the two-port adaptors that were calculated and explored in this chapter are not the only ones that could have been obtained using Eq. 2.28b.

However for the purpose of this thesis the adaptors determined above are sufficient for the examples that have been considered.

Chapter III

PU Realization

3.1 PU Algorithm

In this chapter the PU synthesis algorithm [1], [4] is described. To apply the PU algorithm to a two-port network with polynomials f, g, and h, equations from Section 2.2 are used. After obtaining the elements of the unknown matrix in the first step the interchange of the polynomials f and h for the next computational step is required. At the end of the second extraction block there has to be a QUARL section as described in the previous chapter. The QUARL section reduces the order of the polynomials at each step by one.

Specifically, the two extractions will force the factor z^{-1} in f, g, and h allowing a QUARL to be extracted. In the Figure 3.1 the basic building block for the PU structure with a QUARL section is shown.

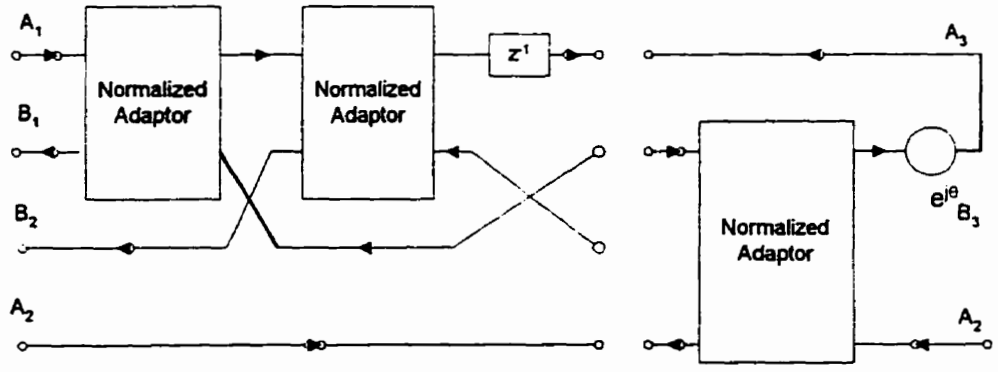

Figure 3.1 Basic Building Block for PU Algorithm with the Final Section

The interchange of the f and h polynomials is in the digital domain whereas in the analog domain it requires two three-port circulators [4].

In the next sections the extraction of the PU building blocks for each of the adaptors that was discussed in the previous chapter will be derived.

3.2 Complex Wave Adaptor From a Real Adaptor and a Unimodular Multiplier

In this section the equations obtained in Chapter 2, namely, Eq. 2.41 and Eq. 2.17 through Eq. 2.23 are used.

The transfer matrix corresponding to Eq.(2.28) with $\phi=0$, $\theta_2=0$ is given by

$$T_a = \frac{1}{\sqrt{1-r^2}} \cdot \begin{pmatrix} e^{j\cdot\theta_1} & -r\cdot e^{j\cdot\theta_1} \\ -r & 1 \end{pmatrix} \tag{3.1}$$

$$(T_a)^{-1} = \frac{1}{\sqrt{1-r^2}} \cdot \begin{pmatrix} e^{-j\cdot\theta_1} & r \\ -r\cdot e^{-j\cdot\theta_1} & 1 \end{pmatrix} \tag{3.2}$$

If $\sqrt{1-r^2} = \sin\theta$ is chosen, it can be seen that

$$(T_a)^{-1} = \frac{1}{\sin\theta} \cdot \begin{pmatrix} e^{-j\cdot\theta_1} & \cos\theta \\ -\cos\theta\cdot e^{-j\cdot\theta_1} & 1 \end{pmatrix} \tag{3.3}$$

Now, the Eq. 3.3 is applied to Eq. 2.19 to obtain polynomials f_b, g_b and h_b.

$$h_b = e^{-j\cdot\theta_1}\cdot h + r\cdot g \ , \quad g_b = r\cdot e^{-j\cdot\theta_1}\cdot h + g \ , \tag{3.4}$$

$$\text{for } h_b(0) = 0 \ , \quad r\cdot e^{j\cdot\theta_1} = \frac{-h(0)}{g(0)} \ \text{ where } r = \left|\frac{h(0)}{g(0)}\right| \ \text{ and } \theta_1 = \arg\left(\frac{h(0)}{g(0)}\right) + \pi. \tag{3.5}$$

Now, after interchanging polynomials f and h for the next step

$$f_{bn} = h_b \ , \quad h_{bn} = f_b \quad \text{and} \quad g_{bn} = g_b \tag{3.6}$$

where subscript n denotes new value of the polynomials used for the next computational step.

V. Cheng [4] has used a different mathematical approach and a starting matrix equation to obtain a real parallel two-port adaptor and extracted a unimodular multiplier section. The reason for pointing this out and extracting equations for the real two-port adaptor is that the results of this thesis can be compared not only to different types of complex two-port adaptors but also to the results that V. Cheng [4] obtained using the equivalent of a normalized ideal transformer for the extraction of PU blocks.

In the next section formulas are derived that are the focal point of this research, the complex cross adaptor in normalized and denormalized form.

3.3 Complex Cross Adaptor-Normalized and Denormalized

From the Eq. 2.28b and the formulas calculated in the previous chapter following is obtained:

$$T = \frac{1}{\sqrt{1 - r^2}} \cdot \begin{pmatrix} 1 & -r \cdot e^{j \cdot \phi} \\ -r \cdot e^{-j \cdot \phi} & 1 \end{pmatrix} \tag{3.7}$$

In Eq. 3.7 T is the transfer matrix of the Normalized Complex Cross Adaptor.

The same steps are used to obtain the inverse of the matrix in Eq. 3.7 as in the previous section.

$$T^{-1} = \frac{1}{\sqrt{1 - r^2}} \cdot \begin{pmatrix} 1 & r \cdot e^{j \cdot \phi} \\ r \cdot e^{-j \cdot \phi} & 1 \end{pmatrix} \tag{3.8}$$

For clear distinction let us label the transfer and inverse transfer matrices as

$$T_{\beta n} \quad \text{and} \quad (T_{\beta n})^{-1} .$$

Using Eq. 2.19 the following is derived

$$T_b = (T_{\beta n})^{-1} \cdot T \tag{3.9}$$

and calculate the polynomials f_b, h_b and g_b in the same fashion as done in the Section 3.2.

$$h_b = h + g \cdot r \cdot e^{j\cdot\phi} \tag{3.10}$$

$$g_b = h \cdot r \cdot e^{-j\cdot\phi} + g \tag{3.11}$$

$$f_b = \sqrt{1 - r^2} \cdot f \tag{3.12}$$

$$\sigma_b = \sigma \tag{3.13}$$

Eq. 3.13 was included just for completeness, but as will be seen in the following sections the only equations of concern are Eq. 3.10 through Eq. 3.12.

The extraction factor for the normalized complex cross wave adaptor is

$$r \cdot e^{j\cdot\phi} = -\frac{h}{g} \qquad \text{for } z^{-1} = 0 \tag{3.14}$$

with the same conditions as in Section 3.2.

All the necessary equations from this section will be implemented in the PU computational algorithm at the end of this chapter with an explanation of the computational steps.

Now, the formula will be derived for the denormalized complex cross adaptor using the same steps as for the normalized one.

The normalized cross adaptor can be represented as a product of two real multipliers and the denormalized complex cross adaptor as shown in Figure 3.2.

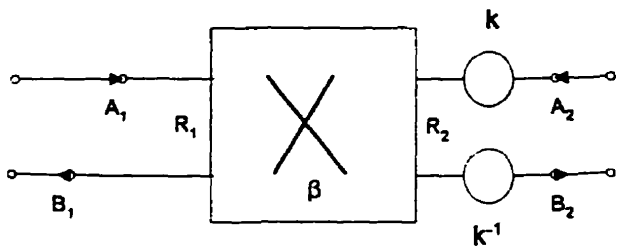

Figure 3.2 Normalized Cross Adaptor Represented by Denormalized Cross Adaptor and Two Real Multipliers

Note: This is useful for the representation of PU building blocks, because the symbolic representation of the denormalized complex cross adaptor has been already defined.

Two diagonal matrices D_1 and D_2 are defined in terms of the two real multipliers:

$$D_1 = \begin{bmatrix} 1 & 0 \\ 0 & \frac{1}{\sqrt{1-r^2}} \end{bmatrix} \quad \text{and} \quad D_2 = \begin{pmatrix} 1 & 0 \\ 0 & \sqrt{1-r^2} \end{pmatrix} \tag{3.15}$$

where $\sqrt{1-r^2} = k$.

The equation of the normalized complex cross adaptor can be calculated from Eq. 3.15 and Figure 3.2.

$$D_1 \cdot S \cdot D_2 = \begin{bmatrix} 1 & 0 \\ 0 & \frac{1}{\sqrt{1-r^2}} \end{bmatrix} \cdot \begin{pmatrix} -r \cdot e^{j\cdot\phi} & 1 \\ 1-r^2 & r \cdot e^{-j\cdot\phi} \end{pmatrix} \cdot \begin{pmatrix} 1 & 0 \\ 0 & \sqrt{1-r^2} \end{pmatrix}$$

$$= \begin{pmatrix} -r \cdot e^{j\cdot\phi} & \sqrt{1-r^2} \\ \sqrt{1-r^2} & r \cdot e^{-j\cdot\phi} \end{pmatrix} \qquad (3.16)$$

Also, it is obvious that $D_1 = (D_2)^{-1}$

These are the equations needed for the different types of PU building blocks.
The next section deals with a review of the Discrete Fourier Transform as a tool that will be used for the representation of the polynomials of the two-ports used in the PU decomposition algorithm.

The formulae for the denormalized two-port adaptor are not given because if satisfactory results are obtained for the normalized cross adaptor, the same rule is in effect for the denormalized complex adaptor represented by the normalized cross two-port adaptor. In other words representation of this adaptor as a part of the PU building block can be

realized in the same fashion as in Figure 3.2 using two real multipliers k and k^{-1}.

3.4 DFT and PU Algorithm

In this thesis the DFT-sample representation of the f, g and h polynomials is used.

For a polynomial $p(z^{-1})$ samples along the unit circle are defined by

$$p_k = p(w^k) \quad , \quad w = e^{-j\cdot 2\cdot\frac{\pi}{N}} \quad , \quad k = 0, 1, \ldots N\text{-}1. \tag{3.17}$$

with N being the degree of the polynomial plus one and the inverse DFT yields the coefficients of the polynomial, specifically the zeroth coefficient

$$p(0) = \frac{1}{N}\cdot\sum_{k=0}^{N-1} p_k \tag{3.18}$$

With DFT-sample procedure order reduction is effected implicitly [4], and hence does not require actual degree reduction.

Now, the PU computational algorithm for the normalized complex cross adaptor using the DFT-sample representation is described.

For the polynomials f, g, h and N the order of the filter plus one, the following algorithm is used:

1. Compute samples on the unit circle

$$f_k = f(w^k) \ , \ g_k = g(w^k) \quad , \quad h_k = h(w^k) \ , \ w^k = e^{-j\cdot 2\cdot\frac{\pi}{N}\cdot k} \ , \ k = 0, 1, \ldots N\text{-}1.$$

2. For the ith extraction step where i goes from 1 to 2N:

Let $r \cdot e^{j \cdot \phi} = \frac{-h(0)}{g(0)}$ which is the extraction factor

where $h(0) = \frac{1}{N} \cdot \sum_{k=0}^{N-1} h_k$ and $g(0) = \frac{1}{N} \cdot \sum_{k=0}^{N-1} g_k$

3. Update all samples as per the derived formulae (:= denotes assignment):

$$f_{kn} := \sqrt{1 - r^2} \cdot f_k$$

$$g_{kn} := h_k \cdot r \cdot e^{-j \cdot \phi} + g_k$$

$$h_{kn} := h_k + g_k \cdot r \cdot e^{j \cdot \phi}$$

$$g_k := g_{kn}$$

where n in the subscript denotes new, calculated values.

4. Interchange f_{kn} and h_{kn} .

5. If i is even, reduce the order of h and f by dividing the DFT samples by w^k

$$h_{kn} = \frac{h_k}{w^k} \quad , \quad f_{kn} = \frac{f_k}{w^k}$$

6. Return to the beginning of the loop at the step number 2 with the next i until

$$i>2\cdot N$$

7. The extraction factor r for i = 2N should be 1.

3.5 Frequency Response Based on the Basic PU Building Block

For the frequency response the same approach is used as in [4]. The frequency response is calculated from the product of 3 by 3 transfer matrices determined from the calculated two-port cross adaptors. This is a direct method of obtaining the frequency response. The PU structure as a product of 3 by 3 matrices is shown in Figure 3.3.

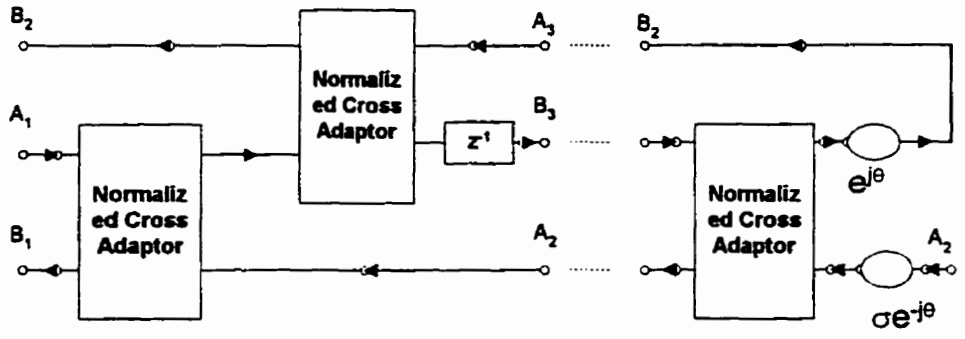

Figure 3.3 PU structure as a product of 3 by 3 matrices

For example if the normalized complex cross adaptor is used then a typical 3 by 3 transfer matrix T_i of the PU building block would be:

$$\frac{1}{\sqrt{1-(r_{2i-1})^2}}\cdot\begin{bmatrix}\sqrt{1-(r_{2i-1})^2} & 0 & 0\\ 0 & 1 & \beta_{2i-1}\\ 0 & \beta_{2i-1} & 1\end{bmatrix}\cdot\frac{1}{\sqrt{1-(r_{2i})^2}}\cdot\begin{bmatrix}1 & \beta_{2i} & 0\\ \beta_{2i} & 1 & 0\\ 0 & 0 & \sqrt{1-(r_{2i})^2}\end{bmatrix}\cdot\begin{pmatrix}1 & 0 & 0\\ 0 & z & 0\\ 0 & 0 & 1\end{pmatrix} \quad (3.19a)$$

To obtain the frequency response of the entire structure the product of all the extraction blocks is needed, namely $T = \prod_{i=1}^{N+1} T_i$ where N is the order of filter and (3.19b)

$$T_{N+1} = \frac{1}{\sqrt{1-(r_{2N+1})^2}}\cdot\begin{bmatrix}\sqrt{1-(r_{2N+1})^2} & 0 & 0\\ 0 & 1 & \beta_{2N+1}\\ 0 & \beta_{2N+1} & 1\end{bmatrix}\cdot\begin{bmatrix}1 & 0 & 0\\ 0 & e^{j\cdot\theta} & 0\\ 0 & 0 & \sigma\cdot e^{-j\cdot\theta}\end{bmatrix} \quad (3.19c)$$

From Figure 3.3 we can see that the last section consists of one two-port cross adaptor and the multiplier section where $e^{j\theta}$ is the multiplier coefficient for the N+1 step.

Also, it is obvious that the final 3 by 3 matrix can be simplified to a 2 by 2 matrix since $A_3 = B_3$.

Using Eq. 2.4a and the given condition the following 2 by 2 scattering matrix is derived:

$$\begin{pmatrix} B_1 \\ B_2 \end{pmatrix} = \frac{1}{T_{22}+T_{21}} \cdot \begin{bmatrix} T_{32}+T_{31} & T_{33}\cdot(T_{22}+T_{31}) - T_{23}\cdot(T_{32}+T_{31}) \\ T_{12}+T_{11} & T_{13}\cdot(T_{22}+T_{21}) - T_{23}\cdot(T_{12}+T_{11}) \end{bmatrix} \cdot \begin{pmatrix} A_1 \\ A_2 \end{pmatrix} \tag{3.20}$$

or

$$\frac{1}{g} \cdot \begin{pmatrix} h & \sigma\cdot f \\ f & -\sigma\cdot h \end{pmatrix} = \frac{1}{T_{22}+T_{21}} \cdot \begin{bmatrix} T_{32}+T_{31} & T_{33}\cdot(T_{22}+T_{31}) - T_{23}\cdot(T_{32}+T_{31}) \\ T_{12}+T_{11} & T_{13}\cdot(T_{22}+T_{21}) - T_{23}\cdot(T_{12}+T_{11}) \end{bmatrix} \tag{3.21}$$

From the Eq. 3.21 the following relationships can be seen:

$$g(z^{-1}) = T_{22}+T_{21} \tag{3.22a}$$

$$f(z^{-1}) = T_{12}+T_{11} \tag{3.22b}$$

$$h(z^{-1}) = T_{32}+T_{31} \tag{3.22c}$$

As discussed in the Chapter 2 based on what the system requirements are, either the frequency response of the transmittance or reflectance is calculated.

The transmittance is given by $\frac{f(z^{-1})}{g(z^{-1})}$ and the reflectance by $\frac{h(z^{-1})}{g(z^{-1})}$.

3.6 Time Domain Representation

In this section the basic building blocks are used for the filter realization in the form of a scattering matrix in order to calculate the frequency response from the time domain.

As shown in Figure 3.3, any filter of given order N can be presented as a structure of N PU building blocks with the N+1th element at the end represented by two complex or two real unimodular multipliers and a two-port adaptor.
If the computational steps of the PU algorithm are accurate the last elements will be unimodular.

In this section a basic block and a final section are used to realize the filter in the time domain. The impulse response is obtained by applying an impulse function at the input and by setting the values in the delays equal to zero. This will give us a general rule and the equations necessary to build a filter of any order using this approach. Of course, any higher order filter would have more computational steps and involve more equations, hence requiring more time. In the next chapter the values of the calculated β coefficients will be used for a 3rd-order complex digital filter and an 8th order filter to obtain the corresponding time domain responses.
To represent a PU building block and the last multiplier in the time domain the z^{-1} delay operator in the digital domain is replaced with a T time domain section in Fig. 3.1 and Fig. 3.3.
Since the normalized complex cross adaptor was used in Fig. 3.3, the focus will be on the realization with denormalized two-ports with two real multipliers.

Note: The Normalized Cross Adaptor is equvalent to the Denormalized Cross Adaptor and two real multipliers.

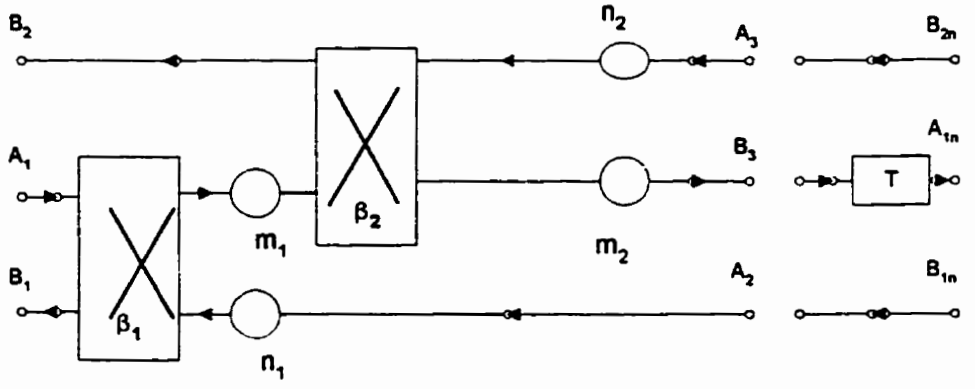

(a)

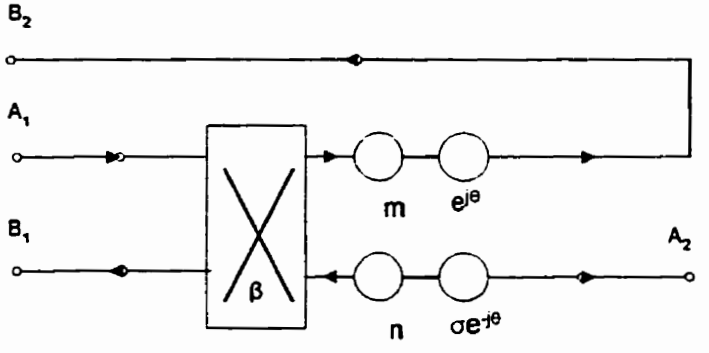

(b)

Figure 3.4 (a) PU Building Block-Time Domain, (b) Final Two-Port Section

Now, for the impulse function at the input, the values for the delays are zeros at a t = 0 and there will be an initial value at the input which will be zero for t = 1, 2, ... n. where t denotes time.

To calculate the necessary values for the circuit from the Figure 3.4a and Figure 3.4b the signal-flow diagram of the complex cross adaptor from the Figure 2.6b is used.

From the Figure 2.6, a matrix equation can be extracted for each PU building block in Figure 3.4a and for the final section from the Figure 3.4b as follows:

$$\begin{bmatrix} b_1 \\ b_2 \\ b_3 \end{bmatrix} = \begin{bmatrix} 1 & 0 & 0 \\ 0 & 1 & 0 \\ 0 & 0 & m_2 \end{bmatrix} \cdot \begin{bmatrix} 1 & 0 & 0 \\ 0 & 0 & 1 \\ 0 & 1 & -\beta_2^* \end{bmatrix} \cdot \begin{bmatrix} 1 & 0 & 0 \\ 0 & 1 & 0 \\ 0 & \beta_2 & 1 \end{bmatrix} \cdot \begin{bmatrix} 1 & 0 & 0 \\ 0 & m_1 & 0 \\ 0 & 0 & n_2 \end{bmatrix} \cdot \begin{bmatrix} 0 & 1 & 0 \\ 1 & -\beta_1^* & 0 \\ 0 & 0 & 1 \end{bmatrix} \cdot \begin{bmatrix} 1 & 0 & 0 \\ \beta_1 & 1 & 0 \\ 0 & 0 & 1 \end{bmatrix} \cdot \begin{bmatrix} 1 & 0 & 0 \\ 0 & n_1 & 0 \\ 0 & 0 & 1 \end{bmatrix} \cdot \begin{bmatrix} a_1 \\ a_2 \\ a_3 \end{bmatrix} \tag{3.23}$$

The quantized values of m_k's and n_k's, where k = 1, 2, ...n+1, must satisfy

$$m_k \le \frac{1}{\sqrt{1 - \left(|\beta_k|\right)^2}} \quad \text{and} \quad n_k \le \sqrt{1 - \left(|\beta_k|\right)^2} \tag{3.24}$$

which utilizes the passive quantization approach for an inverse pair of multipliers as shown by Fettweis [2].

For the final section from the Fig3.4.b, the values for the final m and n are given by Eq.3.24 and for the final multiplier $e^{j\theta}$ the value for the two examples considered in Chapter IV is one. It is important to set up the starting conditions properly and to observe, from the Figure 3.4a, the relation between each of the corresponding values of the PU building blocks, namely:

$$a_3 = b_{2n} \quad \text{and} \quad a_2 = b_{1n} \tag{3.25}$$

where n denotes the new value.

The time domain operation can be explained by using a block diagram. Let p be the highest degree of the given scattering matrix polynomials. Then there are p delays and the structure of the filter realization can be organized as shown in Figure 3.5.

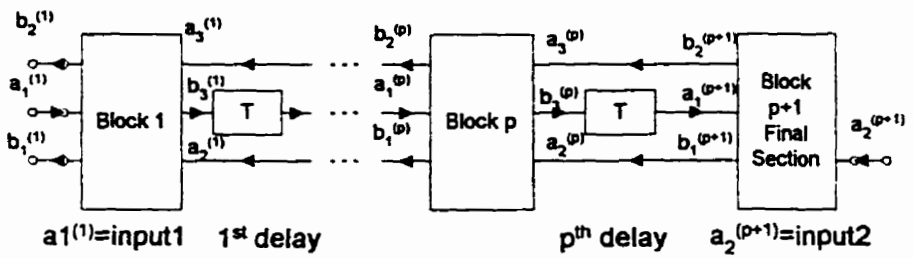

Figure 3.5 Time Domain Block Diagram

For each time instant t, start the calculation with the $p+1^{th}$ block. Then $b_1^{(p+1)}$ and $b_2^{(p+1)}$ are calculated from $a_1^{(p+1)}$ and $a_2^{(p+1)}$ (usually zero) using Figure 3.4b, the flow graph for the cross adaptor Figure 2.6b and the final multipliers, as mentioned earlier in Section 3.6. Next, the calculations determined by block p are carried out in accordance with Figure 3.4a and the flow graph for the cross adaptor.

The inputs are $a_1^{(p)}$ = output of the (p-1)th delay, $a_2^{(p)} = b_1^{(p+1)}$ and $a_3^{(p)}=b_2^{(p+1)}$;

The output $b3^{(p)}$ is the input to the pth delay (which will be the input $a_1^{(p+1)}$ at the next time instant), and outputs $b_1^{(p)} = a_2^{(p-1)}$ and $b_2^{(p)} = a_3^{(p-1)}$ are inputs for block (p-1).

The calculations continue until block 1 is reached where $a_1^{(1)}$ is input1 of the filter. The initial values in the delays are usually set to zero. For the impulse response for the transmittance input1 is set equal to the unit impulse and input2 is set to zero for all times. The frequency response is obtained from the Fast Fourrier Transform of the impulse response at the b_2.

In the next chapter we will give practical examples and realizations with different types of adaptors that were calculated in the Chapters 2 and 3 in the both the digital and the time domains.

Chapter IV

Results and Examples

In this chapter results that are obtained by practical implementation of the formulae from the previous two chapters are presented using a MATLAB software package.

The input data used for the examples presented in this chapter is from V. Cheng's M.Sc. thesis [4], and has been modified to satisfy certain conditions that apply when dealing with complex cross adaptors.

The difference between nominal and quantized values for the coefficients is shown with respect to the output results where quantization was done using 8, 12 and a 16 bit precision for the values of the multiplier coefficients (the betas).

In the next following sections results for an 8th order band-pass filter with real coefficients and a 3rd order band-pass filter with complex coefficients are observed.

Also, the time domain realization of the PU building blocks as explained in Section 3.6 of the previous chapter is discussed. The example of the aforementioned 3rd order complex filter will be observed with regard to the time domain representation.

4.1 The 8th Order Real Band-Pass Filter

For the 8th order filter [4] in this example there was no changes with regards to the input values of the polynomials f, g and h.

The input values for the f, h and g polynomials are given in the Table 4.1.

f zeros	magnitude	angle/pi
constant	0.00090521	0
1	1	0.430034232
2	1	-0.430034232
3	0	0
4	0	0
5	1	0.32053856
6	1	-0.32053856
7	0	0
8	0	0

h zeros	magnitude	angle/pi
constant	0.938442112	0
1	1	0.351732711
2	1	-0.351732771
3	1	0.361097966
4	1	-0.365109797
5	1	0.385182449
6	1	-0.385182449
7	1	0.398308216
8	1	-0.398308216

g zeros	magnitude	angle/pi
constant	0.880673595637835194	0
1	1.008341527656365750	-0.399341528997245882
2	1.008341527656365750	0.399341528997245882
3	1.008545764020980650	-0.350675396462379855
4	1.008545764020980650	0.350675396462379855
5	1.023795851013025390	-0.364509517733878304
6	1.023795851013025390	0.364509517733878304
7	1.023471807530125960	-0.385806739150357242
8	1.023471807530125960	0.385806739150357242

Table 4.1 Input values for the 8th order real band-pass filter

The values for the βs in the polar form and for the quantized βs are given in the Table 4.2.

I	Betas-polar form	angle/pi	Betas-Quantized	angle/pi
1	0.93844211023174	0.00	0.93847656250000	0.00
2	0.00	0.00	0.00	0.00
3	0.38203499663707	1.00	0.38208007812500	1.00
4	0.00	0.00	0.00	0.00
5	0.99487953032633	0.00	0.99487304687500	0.00
6	0.00	0.00	0.00	0.00
7	0.38309650100188	-1.00	0.38305664062500	-1.00
8	0.00	0.00	0.00	0.00
9	0.99585818070986	0.00	0.99584960937500	0.00
10	0.33406509098134	0.00	0.33398437500000	0.00
11	0.36064086441341	1.00	0.36059570312500	1.00
12	0.13647990908653	1.00	0.13647460937500	1.00
13	0.93225326923054	0.00	0.93237304687500	0.00
14	0.95546782599597	0.00	0.95556640625000	0.00
15	0.14097091745874	0.00	0.14086914062500	0.00
16	0.40285264681603	1.00	0.40283203125000	1.00
17	0.01185567766788	0.00	0.01196289062500	0.00
18	1.00000504152195	0.00	1.00000000000000	0.00

Table 4.2. Results for the 8th order filter

An important observation is that angle values for the non-quantized multiplier coefficients (βs) have their values rounded off in this table to -1, 0 or +1. This is valid because the filter is real. Real computational values are slightly different from the rounded values but do not affect the realization of the filter using complex cross adaptors. Now using these values the frequency response, attenuation and magnitude, are presented for the 8th order real band-pass filter using both the nominal and the quantized multiplier coefficients. The values for the inverse multipliers were not given because they are simply calculated from the values of the

corresponding βs.

In the following three figures, Figure 4.1, Figure 4.2 and Figure 4.3, the nominal and the quantized plots for the 8th order example are shown.

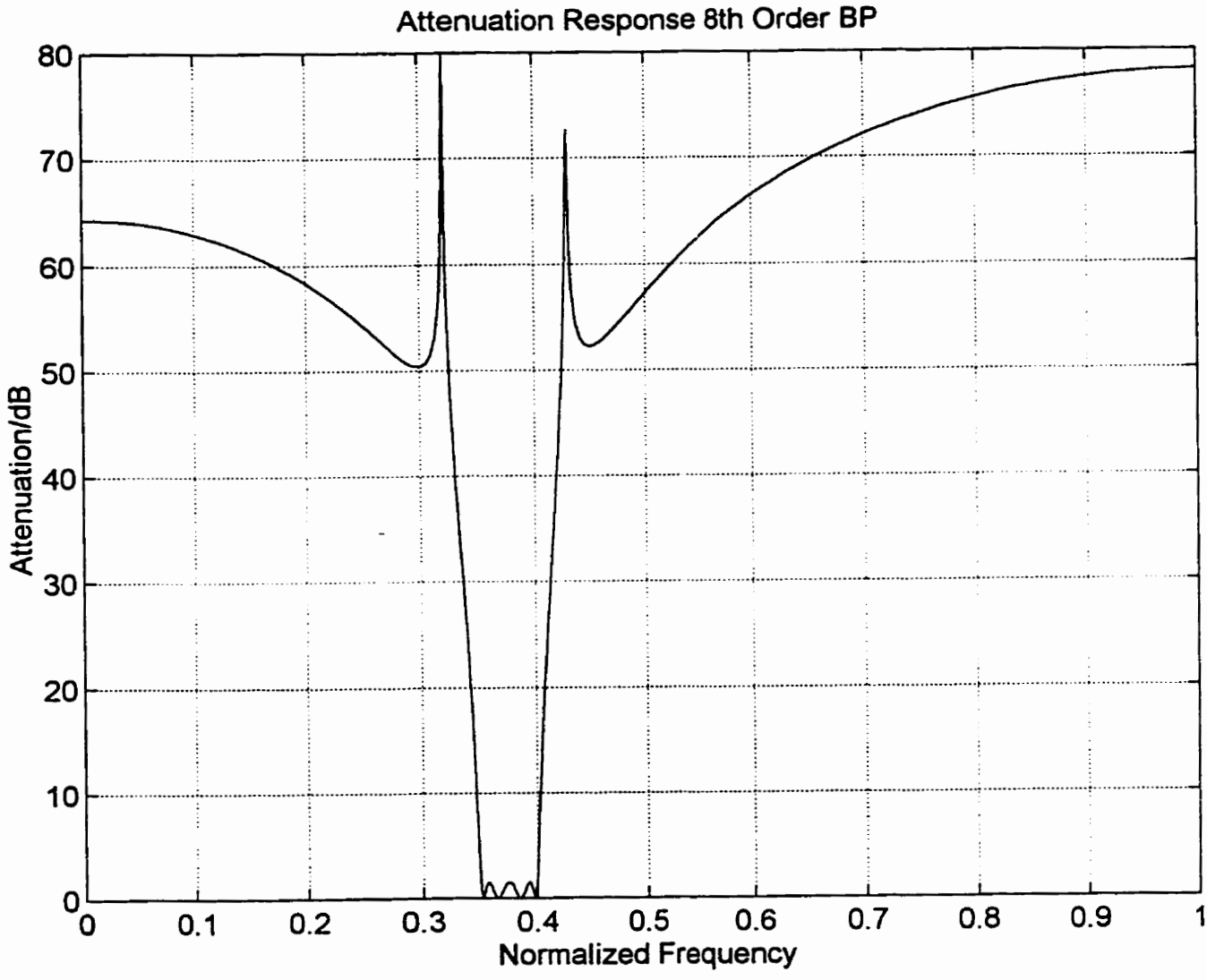

Figure 4.1.a Frequency response plot for the 8th order filter-Quantized to 12 bits

In the following figure we give the nominal frequency response.

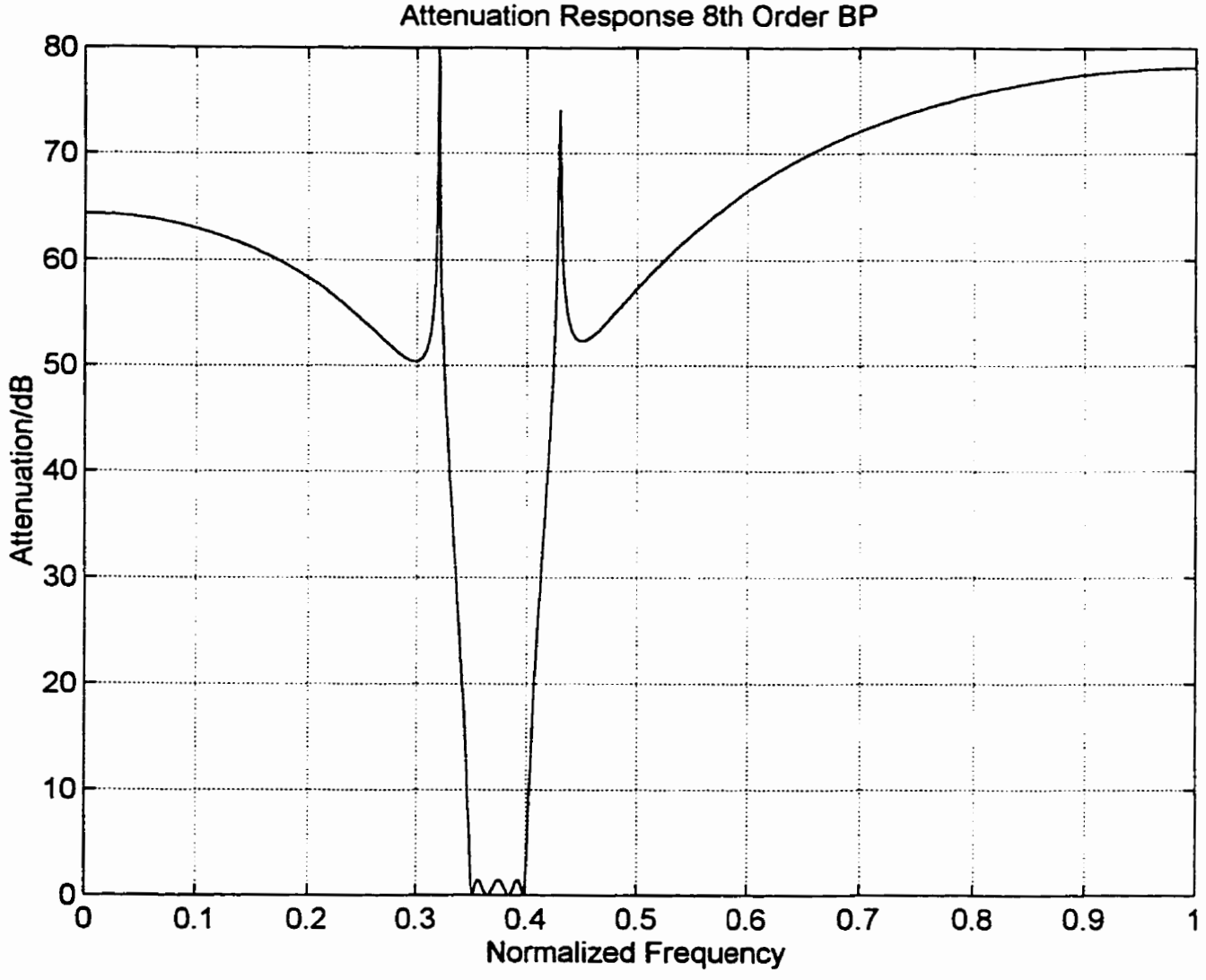

Figure 4.1.b Frequency response plot for the 8th order filter-Nominal

In the following figure the frequency response with the 16-bit precision is shown. For each of these plots 800 discrete time instances were collected.

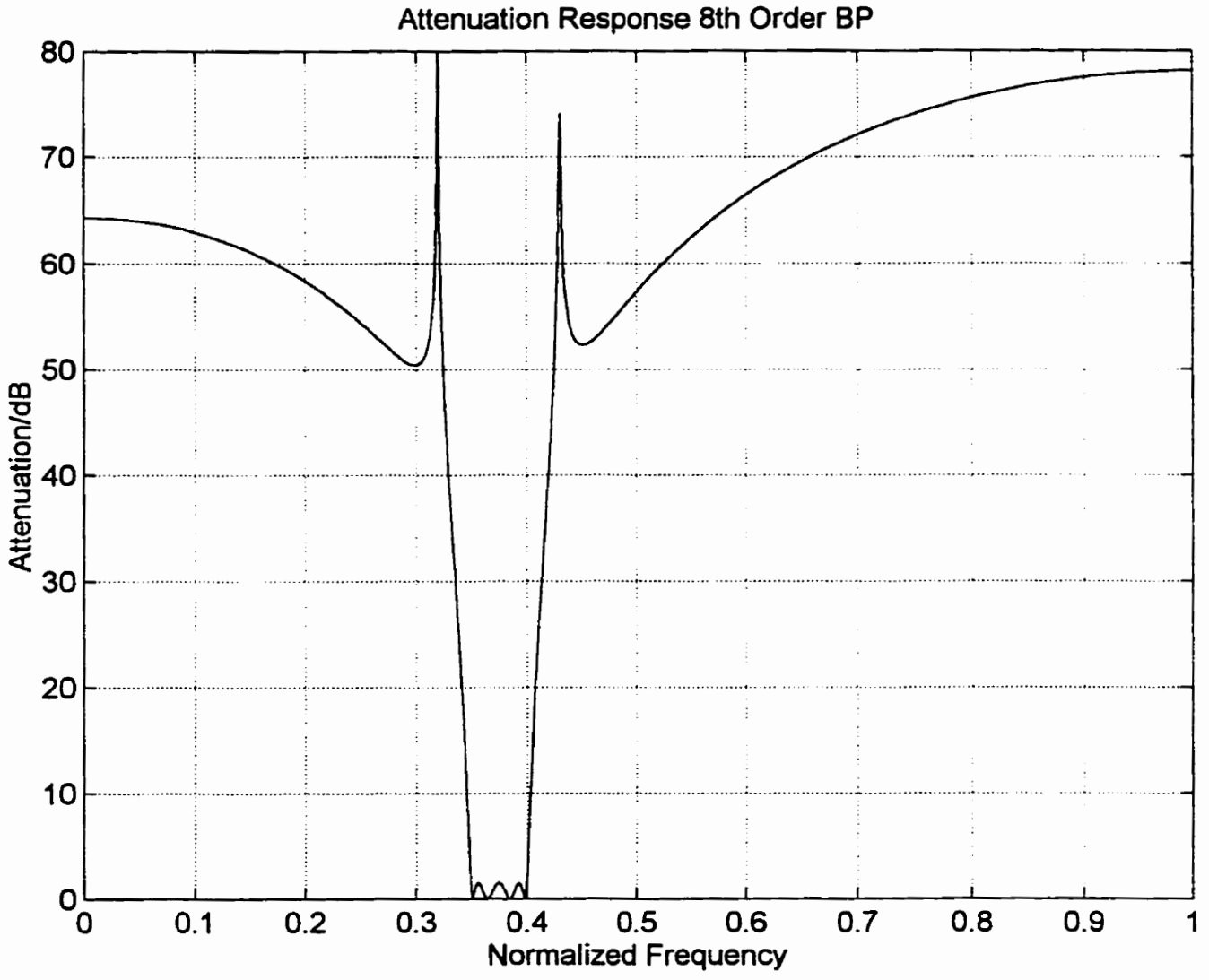

Figure 4.1.c Frequency response plot for the 8th order filter-Quantized to 16 bits

The last frequency response shown has 8-bit precision. It is obvious that for the value of the transmission zero the attenuation value is different than for the other three plots.

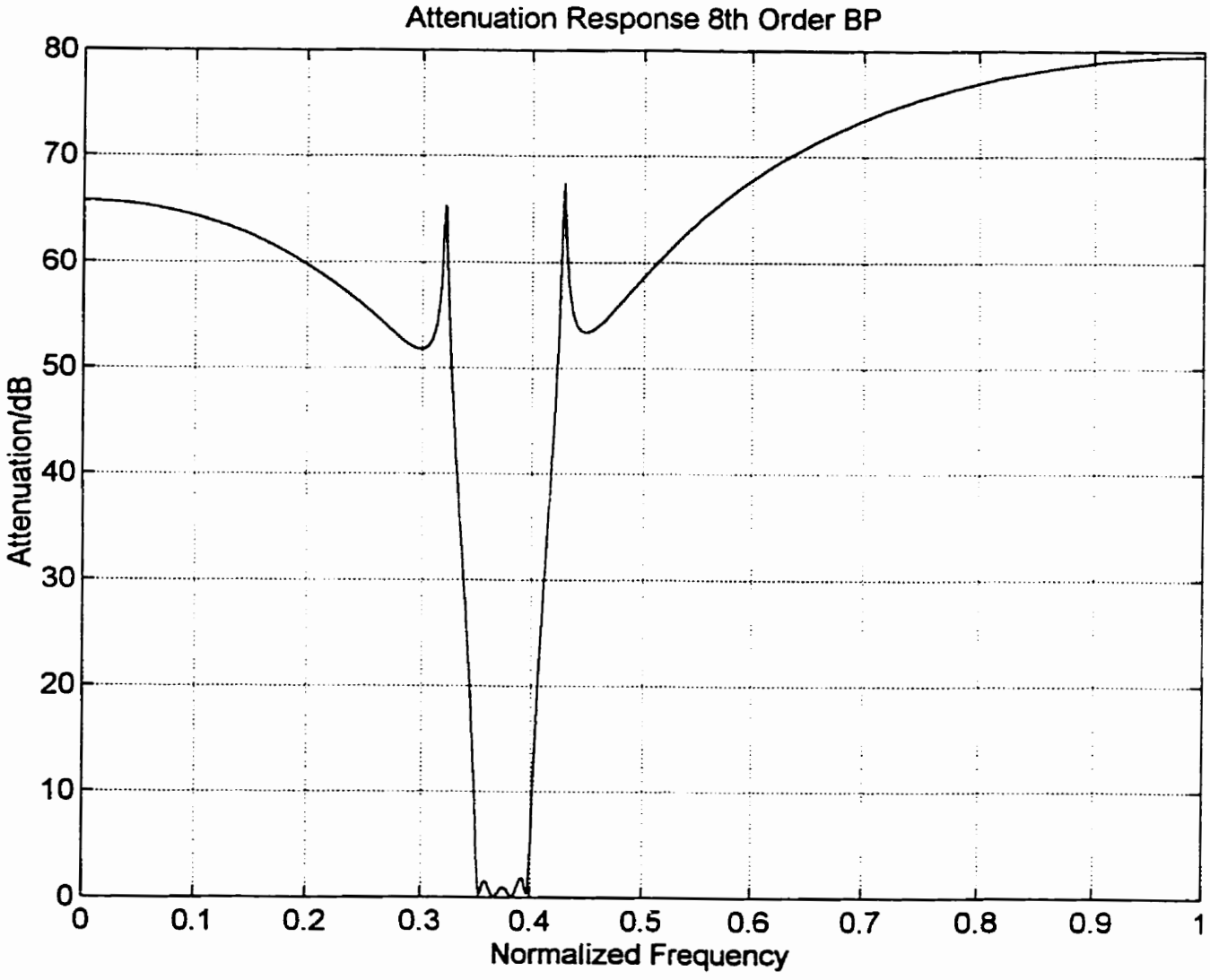

Figure 4.1.d Frequency response plot for the 8th order filter-Quantized to 8 bits

The important difference can be seen when the ripples for both quantized and nominal plots are compared because the quantized one is no longer lossless regardless of the number of the bits.

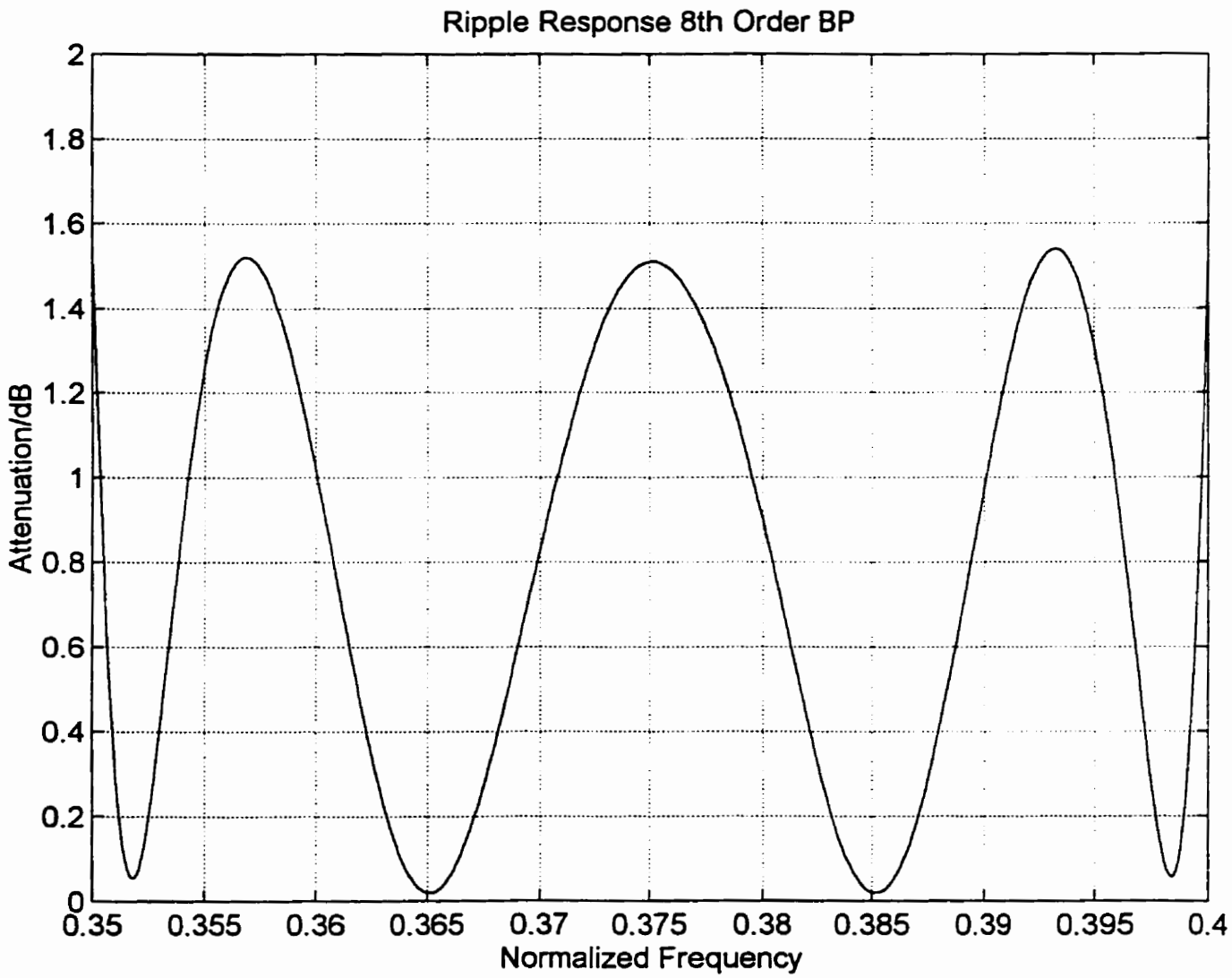

Figure 4.2a Ripple response for the 8th order filter-Quantized to 12 bits

It is obvious from Figure 4.2.a that after using quantized coefficients the ripple plot represents the ripple of a lossy filter. After seeing the figure with the nominal value this is obvious.

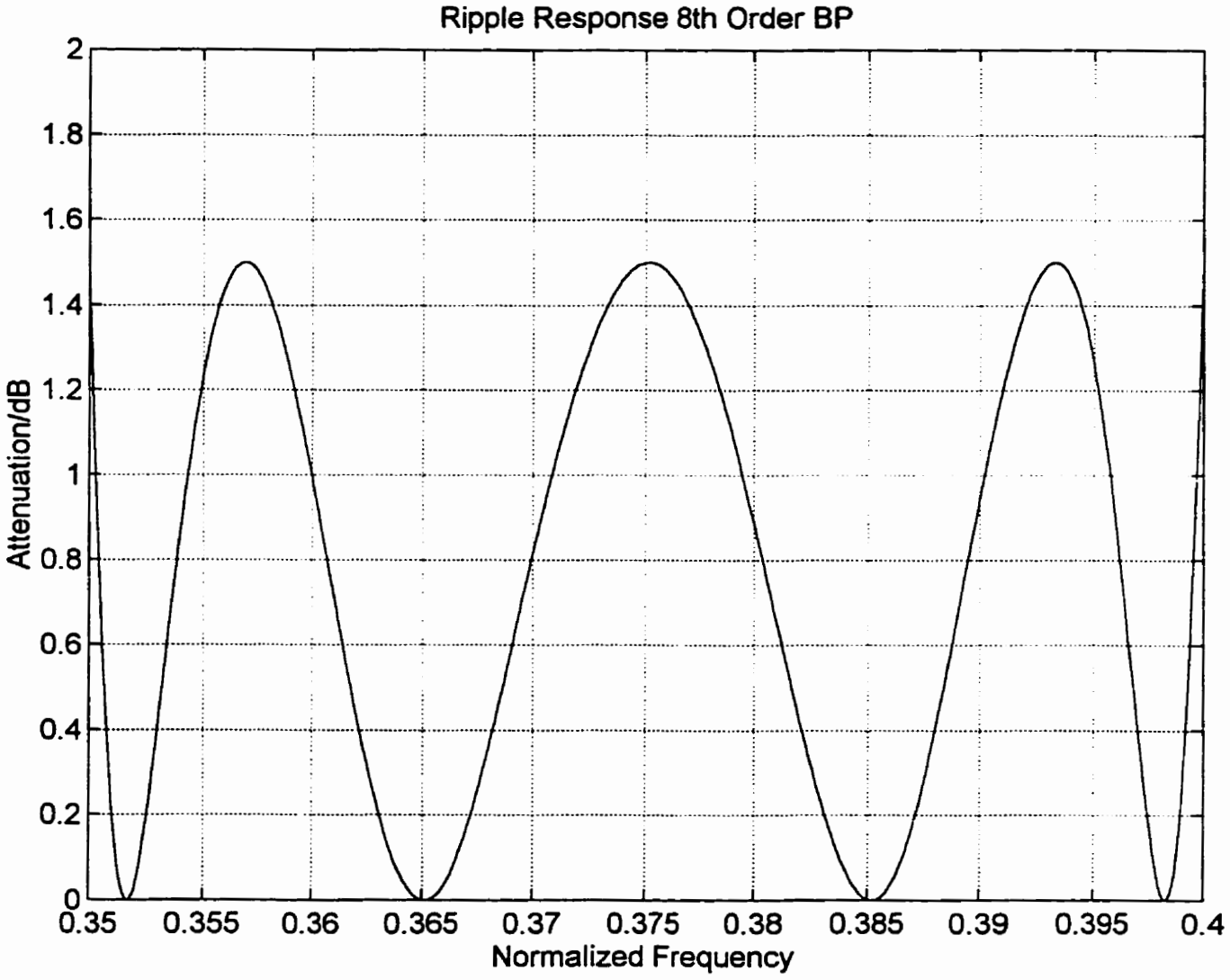

Figure 4.2.b Ripple response for the 8th order filter-Nominal

Figure 4.2.c represents the ripple using quantized coefficients with the 16-bit precision, hence obtaining the ripple plot closer to the nominal value than the 12-bit one, but the difference is not very noticeable.

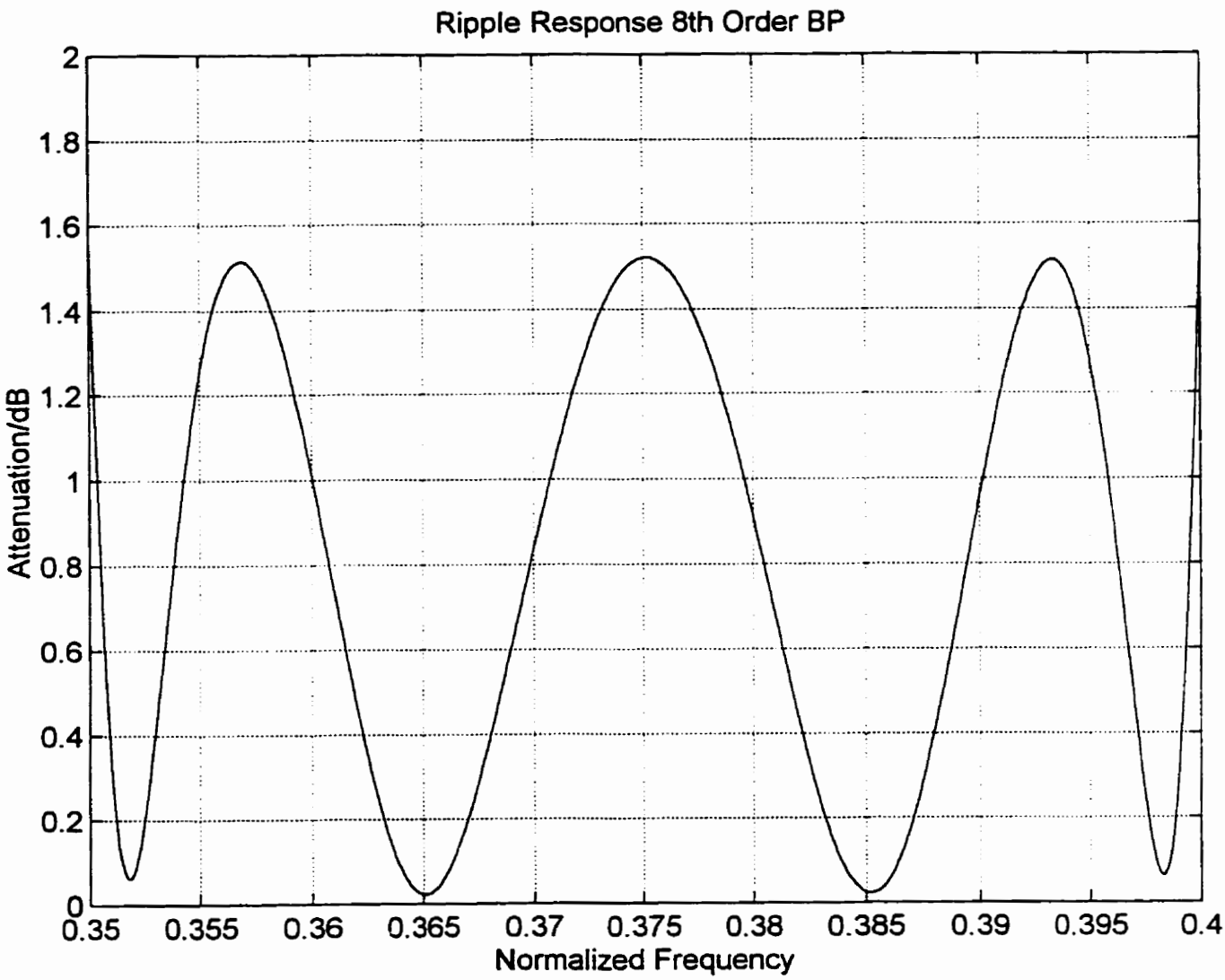

Figure 4.2c Ripple response for the 8th order filter-Quantized to 16 bits

Figure 4.2.d represents the ripple using quantized coefficients with 8-bit precision, and the ripple plot derived is much lossier than the other two plots with the quantized coefficient values.

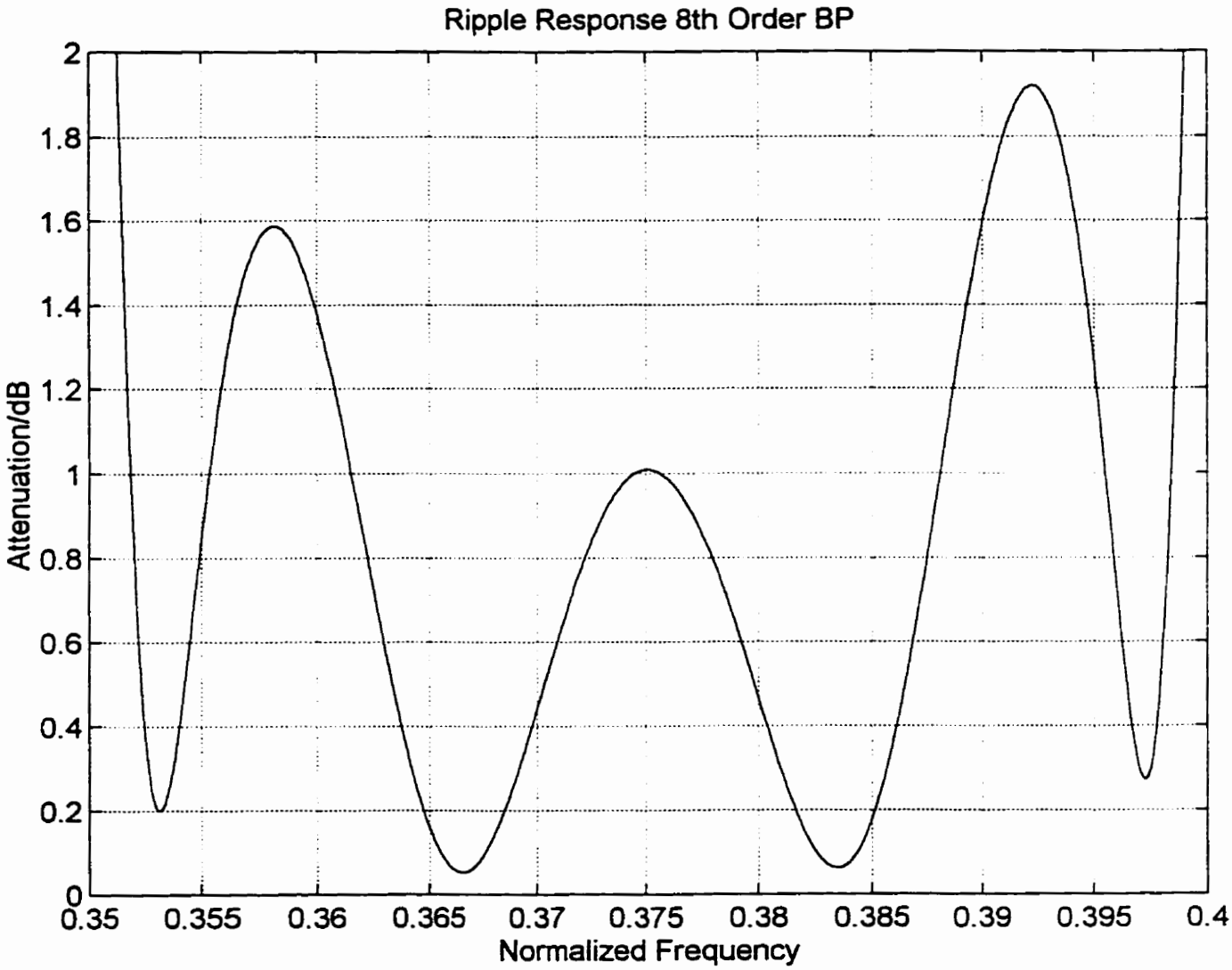

Figure 4.2d Ripple response for the 8th order filter-Quantized to 8 bits

The difference between these plots and plots obtained in [4] is a noticeable one with regard to the ripple plots, where even 8-bit precision for the cross adaptor in this thesis gave better results than 12-bit precision in [4].

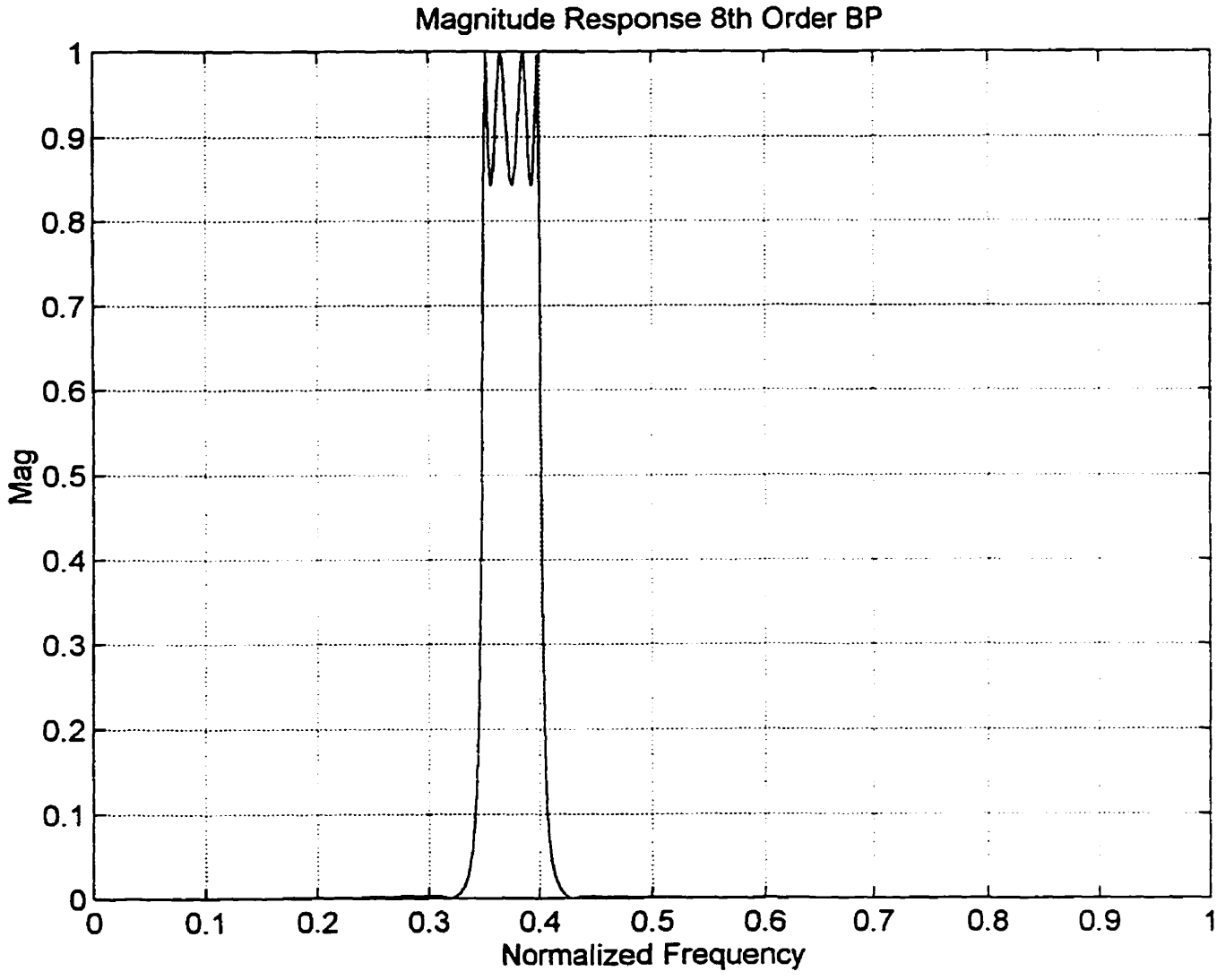

Figure 4.3 Magnitude representation for the 8th order filter

Also, for the 8-bit precision in [4] the program terminated abruptly requiring recalculation of f, g and h with higher precision whereas this program gave satisfactory results.

4.2 The 3rd Order Complex Band-Pass Filter

For the 3rd order complex filter input values for the f, g and h were changed slightly from those in [4].The f constant was set to 1 and the constant factors of h and g were scaled accordingly. In addition, the phase of g was modified to make the final multiplier in the realization equal to one. The input values for the f, h and g polynomials are given in the Table 4.3.

f zeros	magnitude	angle/pi
constant	1	0
1	1.2395398055922130300	-0.35250172859245779120
2	6.5571344746207005200	-0.32828367713287778720
3	0.9737902670856363880	-0.38138581580702775920

h zeros	magnitude	angle/pi
constant	551.21541611546160320	-0.11737612550597118200
1	1	-0.34615340690000000020
2	1	-0.31883573410000000020
3	1	-0.36435118300000000020

g zeros	magnitude	angle/pi
constant	527.83556101667584810	0.0293412000
1	1.0340581281849684080	-0.31527422385588782490
2	1.0416657544134990300	-0.34774492509166970300
3	1.0124727238645185820	-0.36632202873911906100

Table 4.3 Input values for the 3rd order complex band-pass filter

The values for the coefficients and for the quantized coefficients are given in the polar form in the Table 4.4.

I	Betas-polar form	angle/pi	re{β} Quantized 12 bits	im{β} Quantized 12 bits
1	0.957560092158142	-0.1467164718192946	0.857666015625	0.425781250000
2	0.04770248295612563	-0.0621712438456876	0.046875000000	0.009277343750
3	0.9982523291165384	-0.8088364869473473	-0.823486328125	-0.564208984375
4	0.101258747195149	-0.2819933514063858	0.063964843750	-0.078369140625
5	0.9942150314273052	0.5332730477632998	-0.103759765625	0.988769531250
6	0.9147984726785162	0.6187713663468710	-0.334960937500	0.851806640625
7	0.3146996680549092	-0.3226698425773926	0.166503906250	-0.267089843750
8	1.002913755688828	-0.0000558942372640	1	0.00

Table 4.4 Results for the 3rd order complex filter

As can be seen, the difference between this and the previous example is that angles are no longer ones and zeros and have non-zero values.

Now, as in the previous section, these results are used to obtain the necessary plots.

In the following three figures, Figure 4.4, Figure 4.5 and Figure 4.6, we present the attenuation versus frequency plot, ripple and magnitude plots for the 3rd order complex filter.

Also, the frequency response and the ripple for the nominal values of coefficient and the corresponding magnitude is shown because, as for the 8th order real filter example, the only noticeable difference is for the ripple frequency response, where the nominal value represents a lossless filter and the quantized one represents a lossy one but for consistency in this thesis all three plots are included.

In the next figure we give the frequency response of the 3rd order complex filter with the quantized values for the coefficients with 12-bit precision and the same number of instances as for the 8th order real filter.

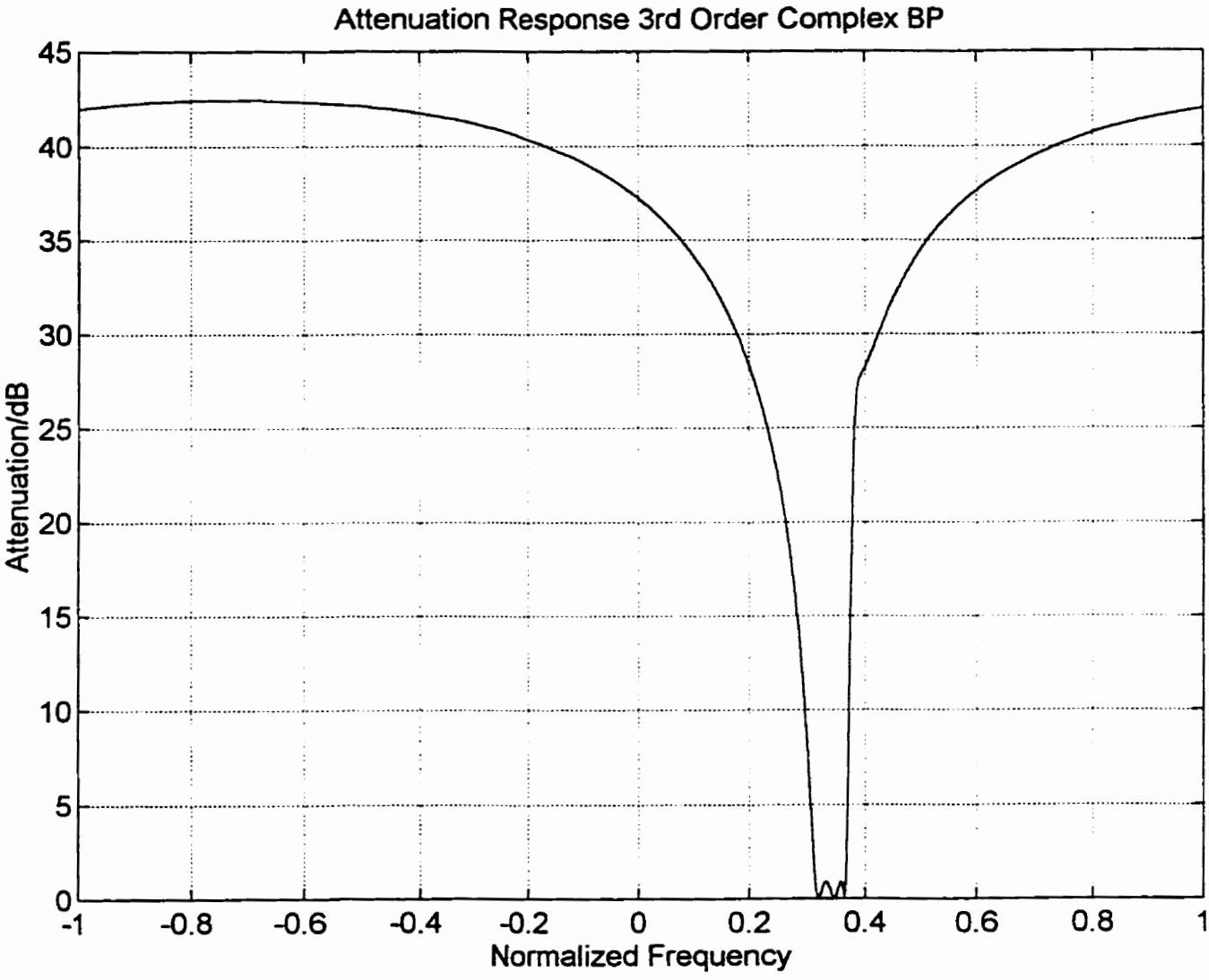

Figure 4.4a Frequency response for the 3rd order complex filter-Quantized to 12-bits

In the Figure 4.4b the frequency response of the 3rd order complex filter with the nominal values for the coefficients is shown and the difference between this one and the quantized ones is not significant as expected.

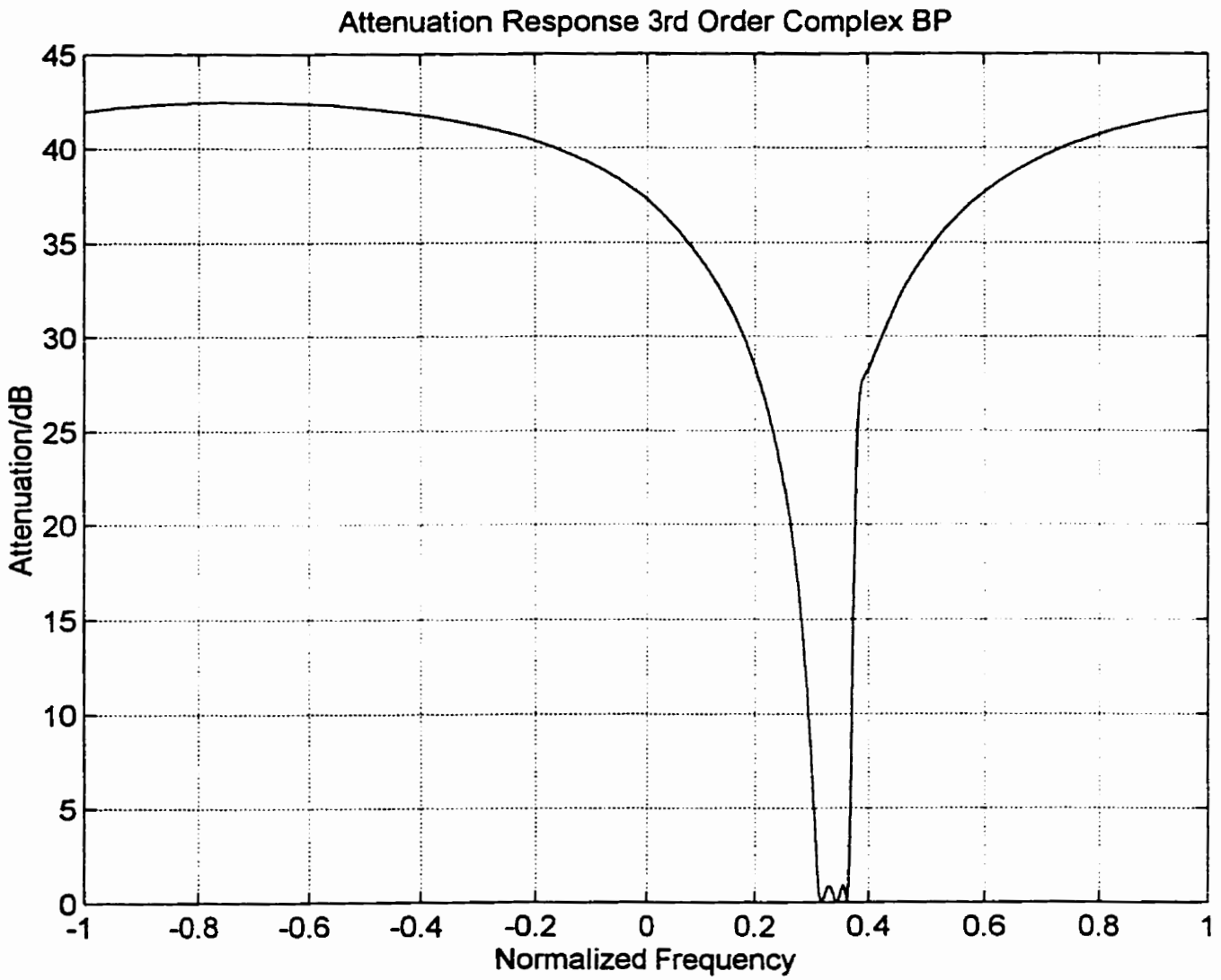

Figure 4.4b Frequency response for the 3rd order complex filter-Nominal

In the Figure 4.4c the frequency response of the 3rd order complex filter with the quantized values for the coefficients with 16-bit precision is shown, and as discussed no significant change was noticed.

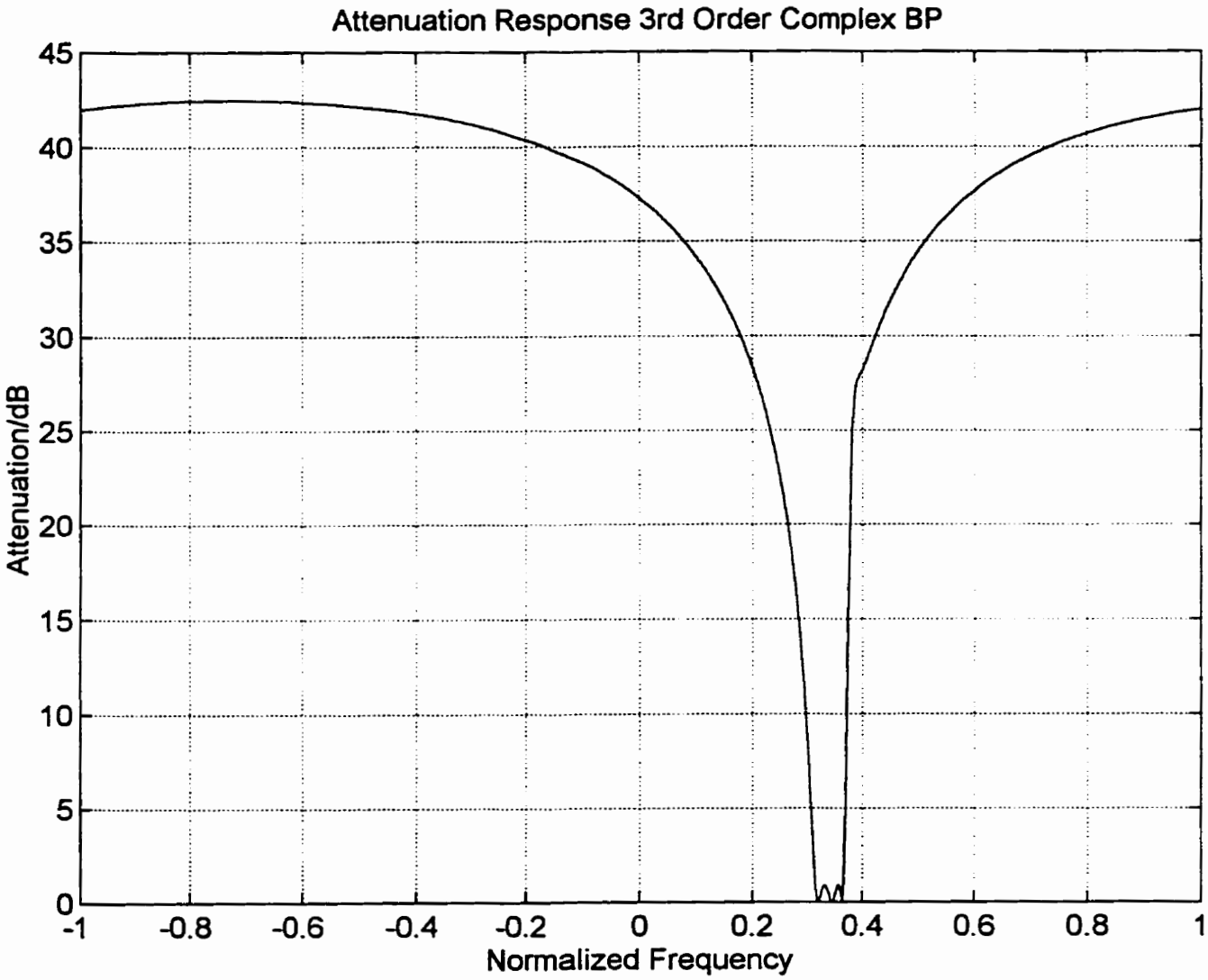

Figure 4.4c Frequency response for the 3rd order complex filter-Quantized to 16-bits

For the 8ht order filter when 8-bit precision was used for the values of the quantized coefficients, the frequency response had different values at the transmission zero points. With the 3rd order filter this is not the case.

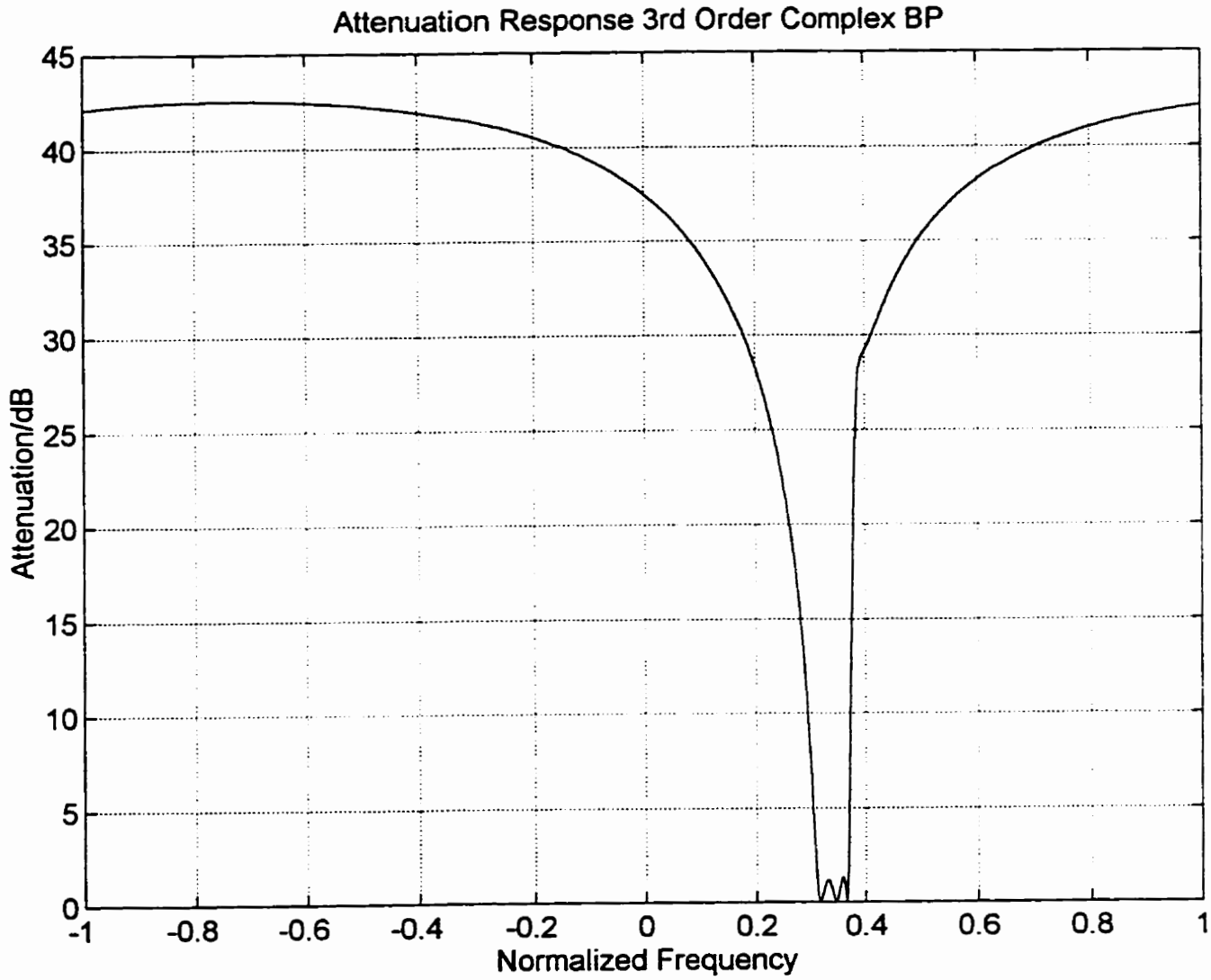

Figure 4.4d Frequency response for the 3rd order complex filter-Quantized to 8-bits

In Figure 4.4 we have obtained the same frequency response as in [4] except that for the passband in this thesis (the quantized ripple) for the complex cross adaptor gives better results than in [4].

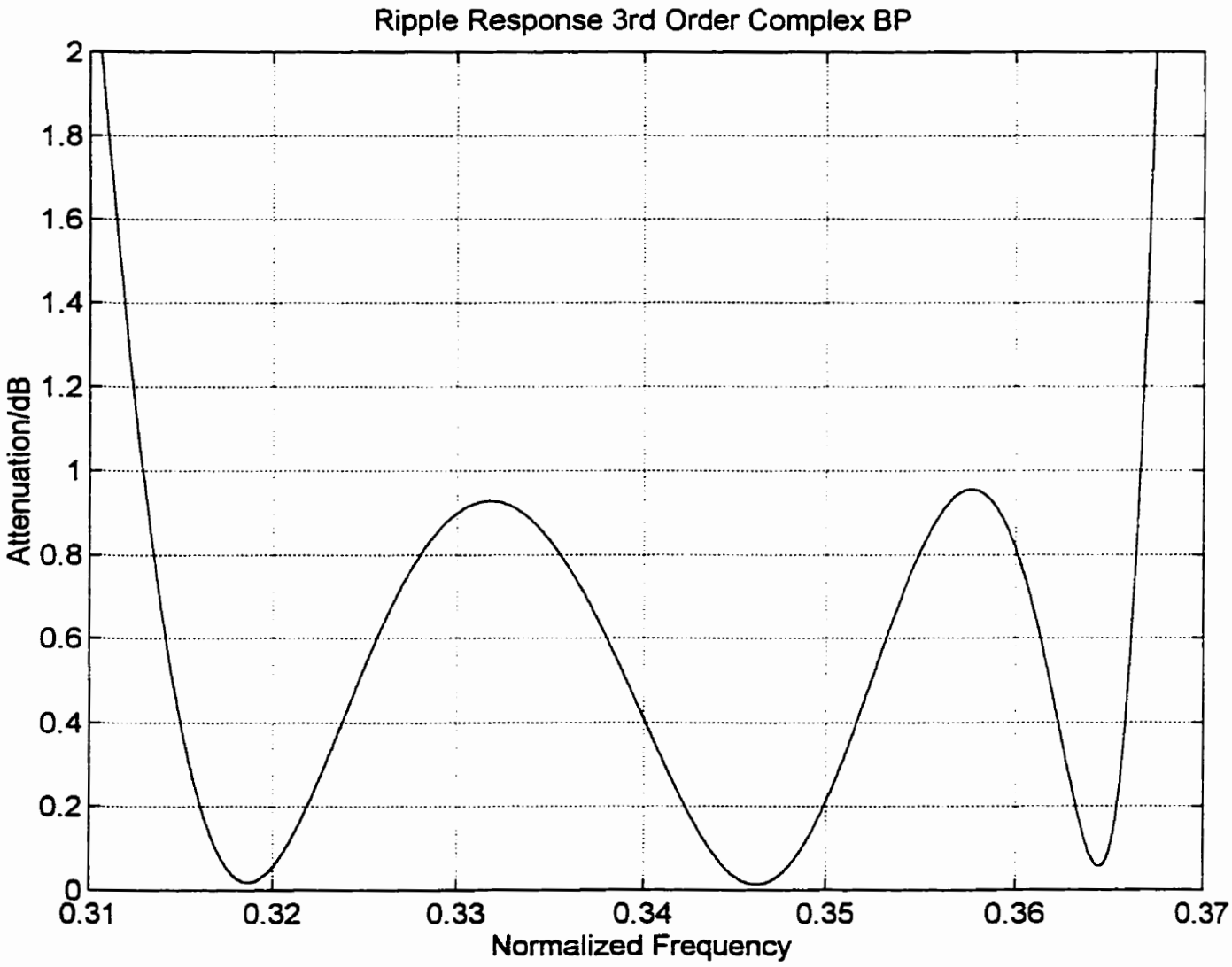

Figure 4.5a Ripple response for the 3rd order filter-Quantized to 12-bits

As for the 8th order filter, the ripple response of the 3rd order filter obtained using the nominal value of the coefficients is shown for the purpose of comparison with the ripple plots obtained using quantized values of the coefficients.

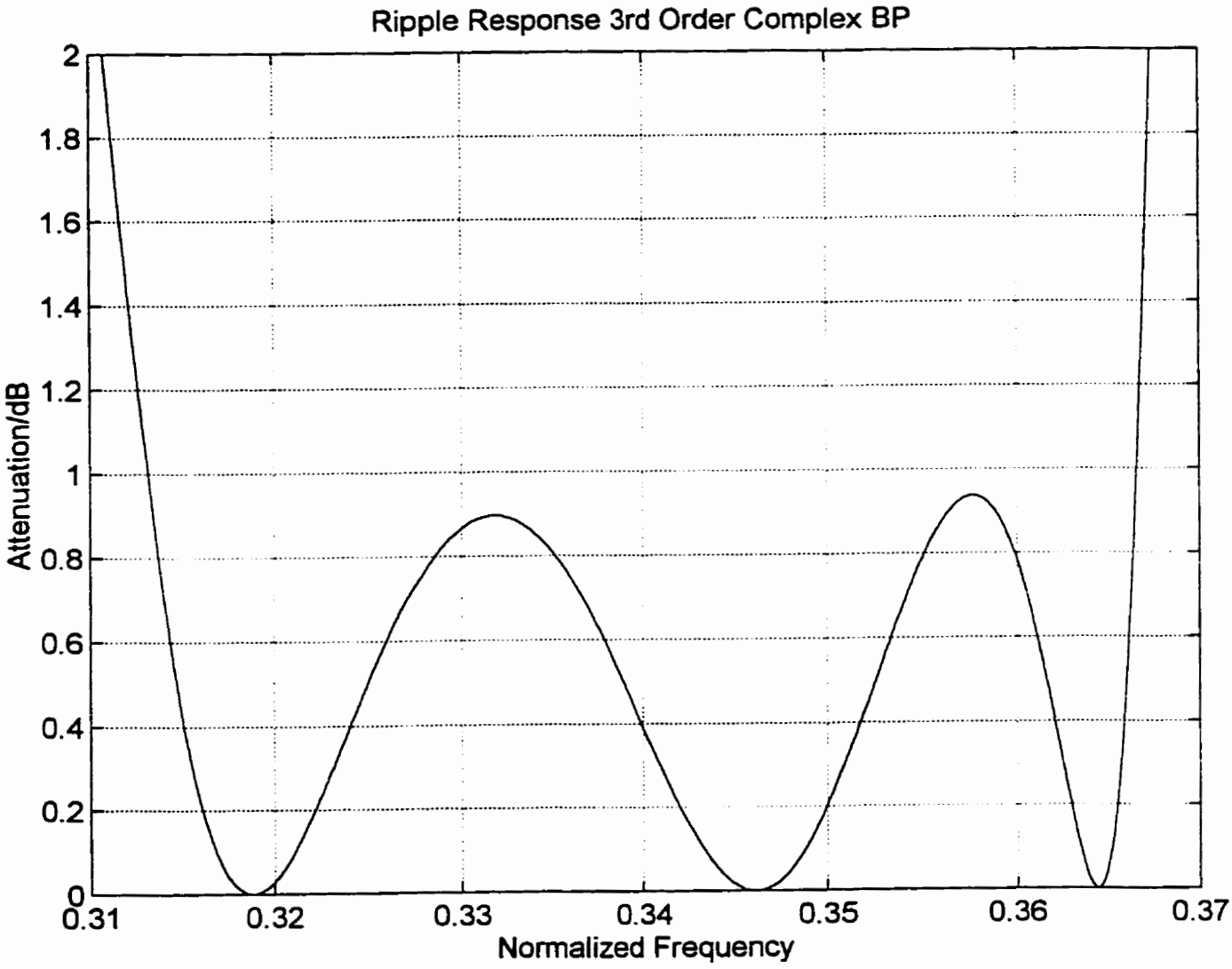

Figure 4.5b Ripple response for the 3rd order filter-Nominal

The ripple plot with 16-bit precision shown in Figure 4.5c is not significantly different from the 12-bit precision plot.

The difference is noticeable when compared to the ripple plot using nominal values.

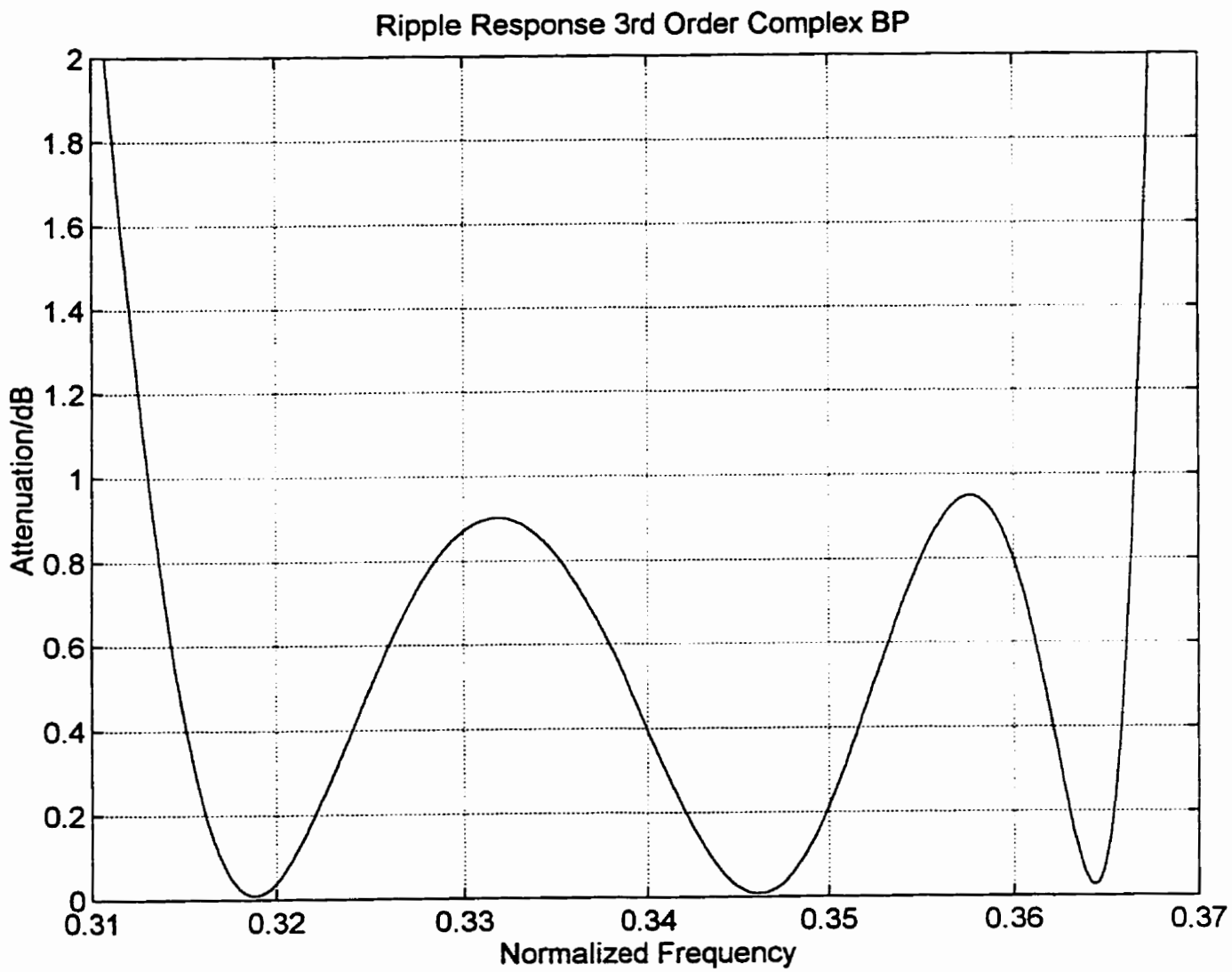

Figure 4.5c Ripple response for the 3rd order filter-Quantized to 16-bits

The ripple plot with 8-bit precision shown in Figure 4.5d differs from both quantized and nominal plots significantly, both by shape and by the lossiness.

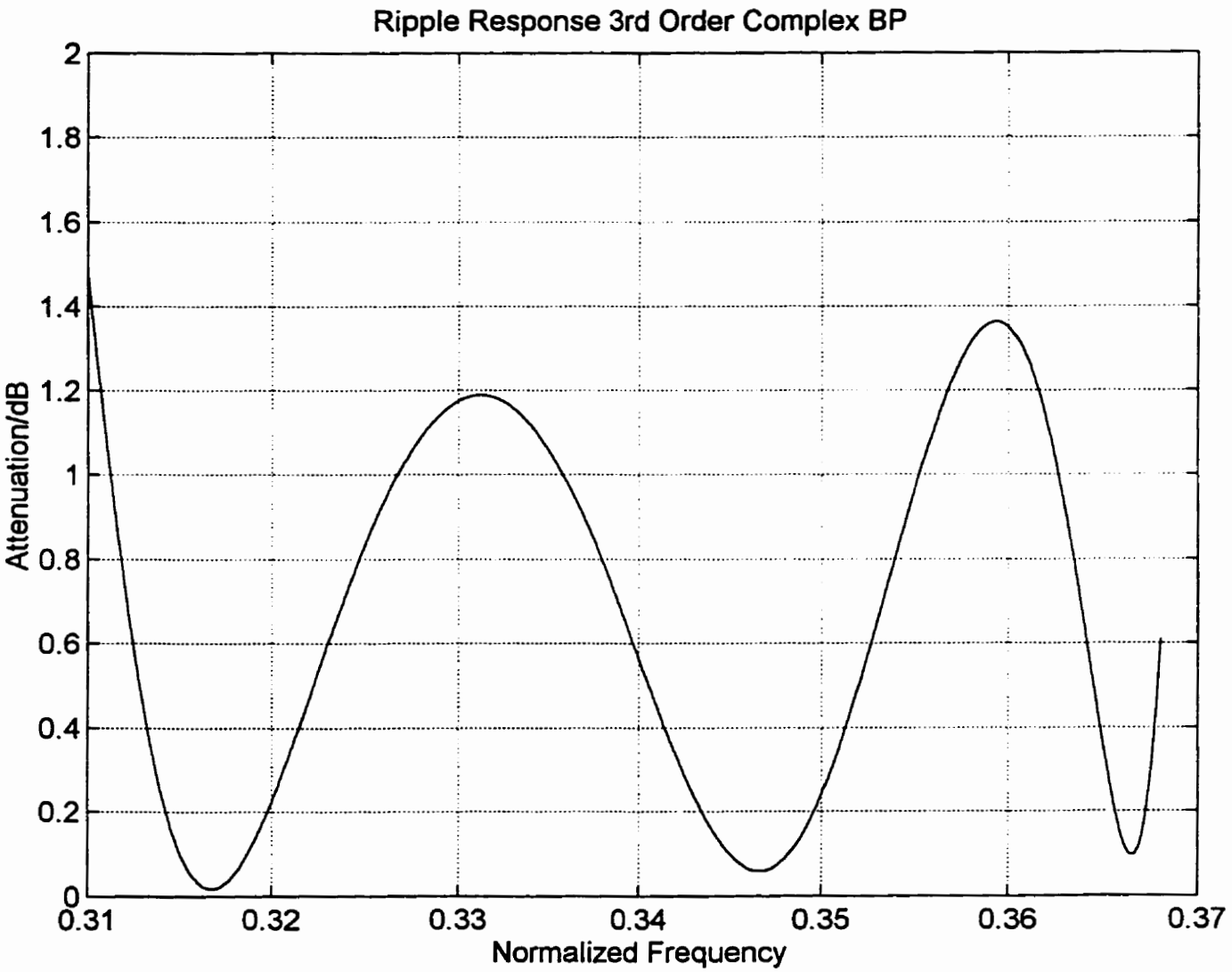

Figure 4.5d Ripple response for the 3rd order filter-Quantized to 8-bits

The last figure given for this example is the magnitude response of the 3rd order complex filter.

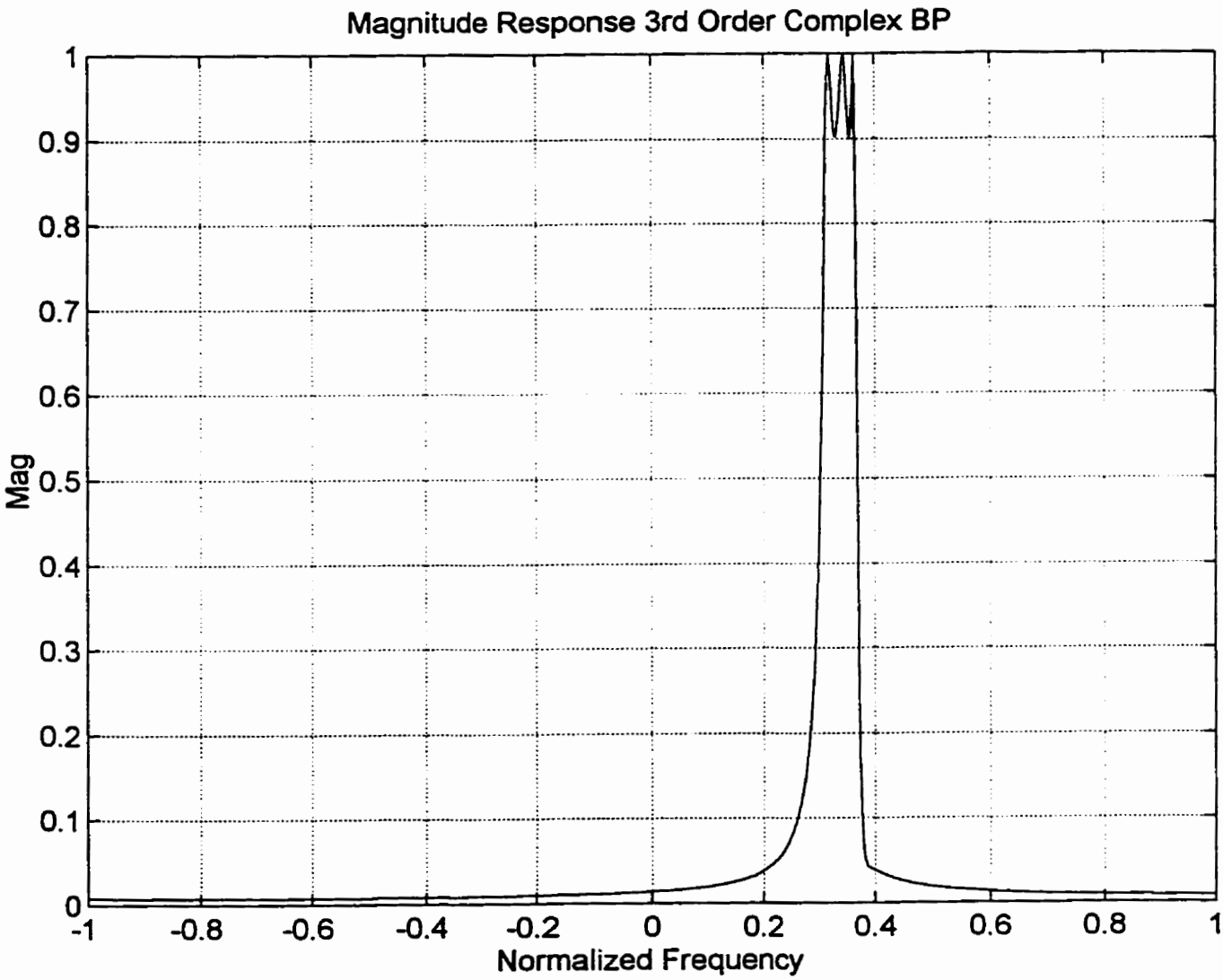

Figure 4.6 Magnitude response for the 3rd order complex filter

Further discussion and comparison with results obtained in [4] and a sensitivity issues will be provided at the end of this chapter.

The conclusion based on the previous two chapters is that the complex cross adaptor gives good results after using quantized values of the multipliers (βs) and the inverse multiplier pairs. Further discussion will be given in the next chapter.

4.3 Time Domain Realization and the Examples

In this section the approach determined in Section 3.6 is used and applied to the 3rd order complex filter and an 8th order filter observed in the previous section in an attempt to obtain the time domain response of the given filter using the PU building blocks from Figure 3.4.a and Figure 3.4.b. A general computational algorithm was designed that was used in this section to obtain the result regardless of the filter order or the polynomials of the lossless filter.
The same coefficients are used for both methods of obtaining the frequency responses of the 8th and 3rd order digital filters. The frequency response that was obtained, based on the unit sample applied at the input of each of the filters produced ripple characteristics similar to those obtained in Sections 4.1 and 4.2.
Note: Since the attenuation and magnitude frequency responses for the time domain were essentially the same as those of the digital domain we will not present their plots.
As mentioned above, both plots for the digital and the time domain were made using the quantized coefficients.

In the next figure the ripple frequency response of the 8th order real band-pass filter is given.

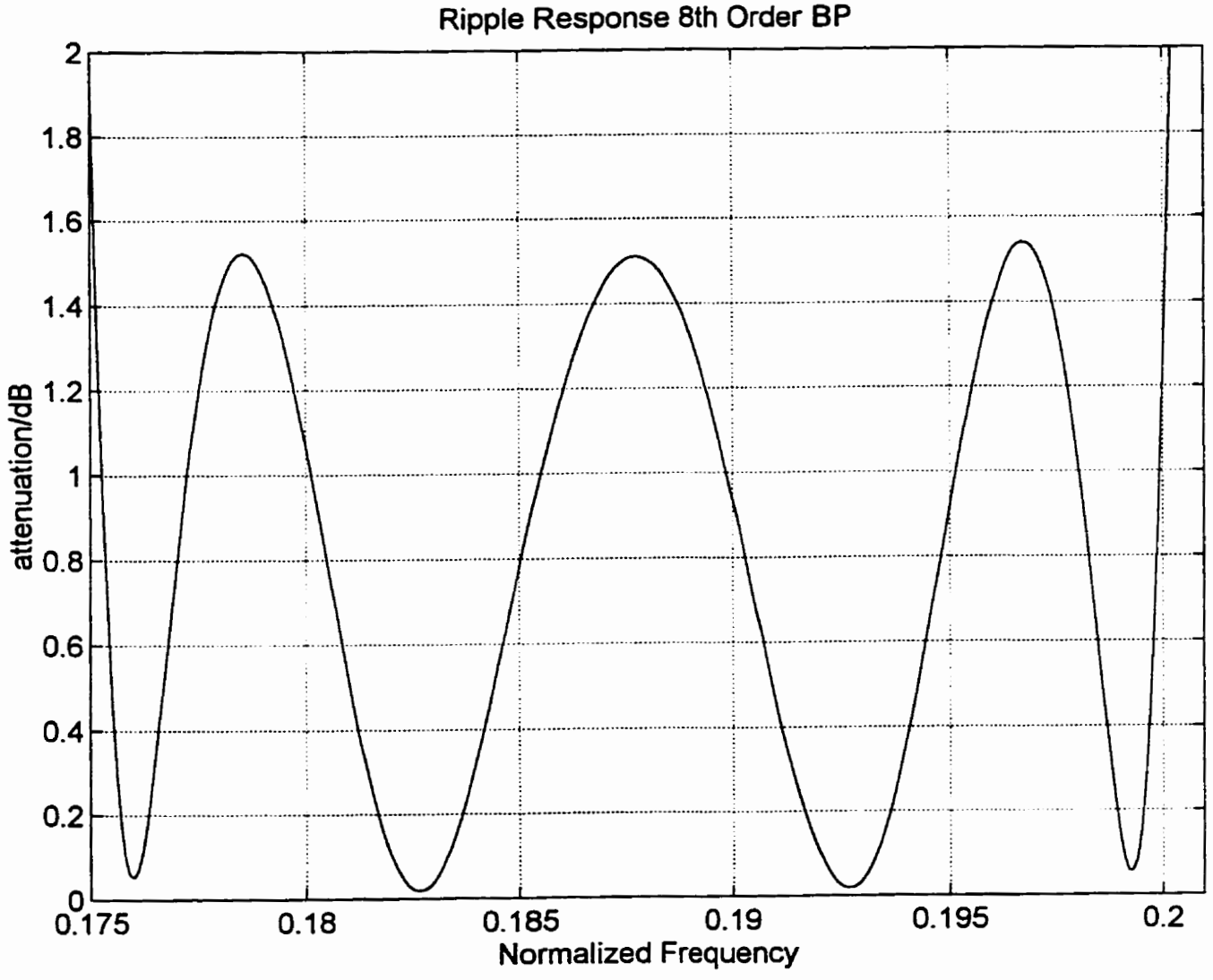

Figure 4.7.a Ripple response for the 8th order filter-Time Domain (12 bits)

The final plot of this chapter has been presented in the next figure which represents the ripple frequency response of the 3rd order complex filter.

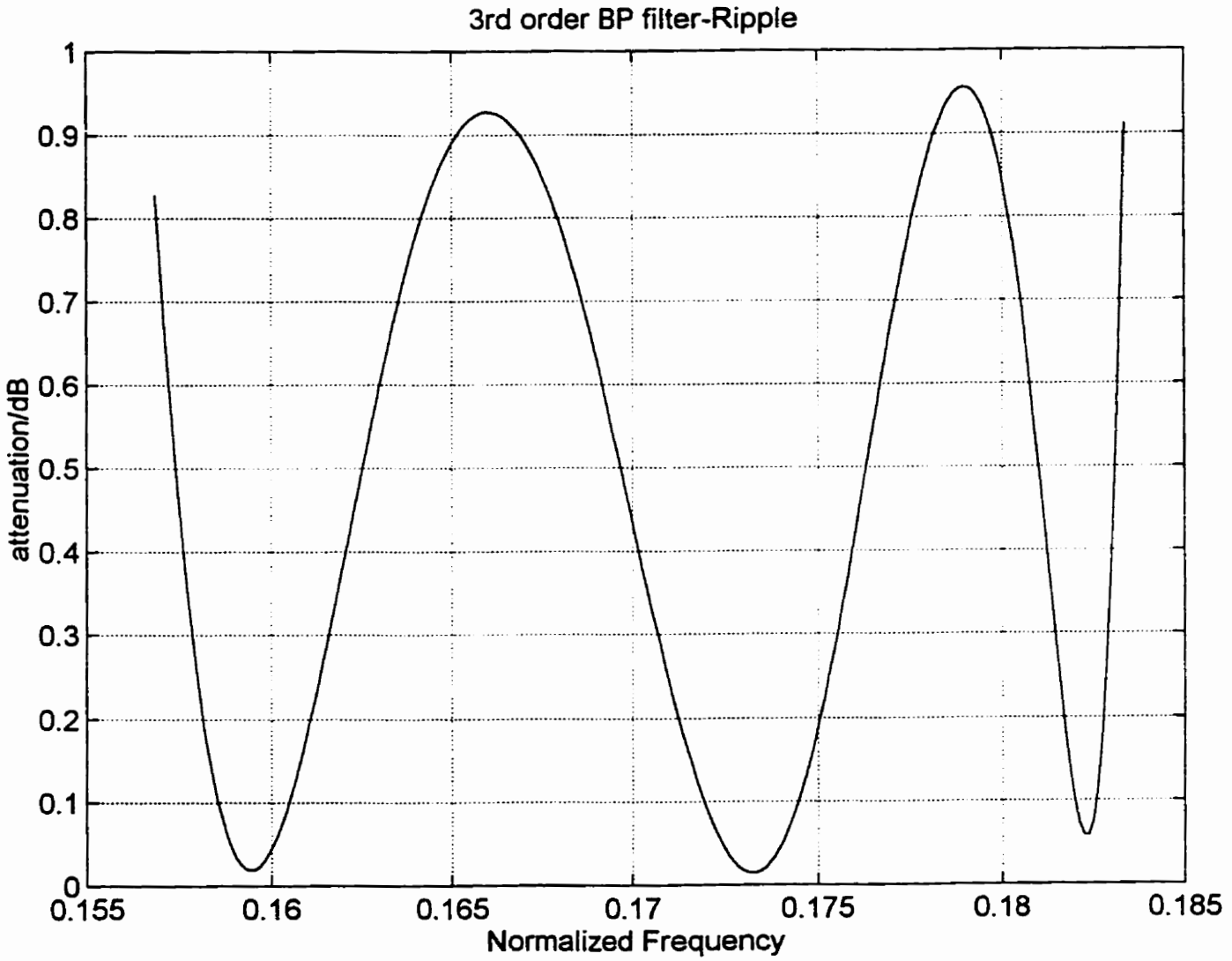

Figure 4.7.b Ripple response for the 3rd order complex filter-Time Domain (12 bits)

As mentioned above, the time domain ripple frequency response with the quantized multiplier coefficients (βs) resembles the nominal values of the digital filters from the previous two sections of this chapter.

With regard to the results from Sections 4.1 and 4.2 the following was concluded:

1. Using the quantized coefficients with 8-bit precision shows deviation from the higher quantized values and the nominal one. When this result is compared to the result from [4] it is satisfactory allowing even for the 8-bit implementation.
2. The filter realized using cross adaptor in the PU algorithm is less sensitive than the realization presented in [4].

In the next chapter the final conclusions are presented based on the findings and the results obtained from the previous chapters and materials mentioned in the reference section. Also, a discussion of pipelineability will be given and the possible practical implementation of the above results and formulae in the fields of VLSI and DSP.

Chapter V

Conclusions

A realization structure and a design for complex and real lossless two-port filters using the PU structure was given. The implementation of the PU blocks using the complex cross adaptor was used. The advantage over other techniques using two-port adaptors [4] was that only one coefficient was used in the realization of the adaptor.

Two types of the complex cross adaptors were used, both normalized and denormalized.

It is important to notice that the denormalized adaptor was used with two real multipliers as a equivalent of the normalized adaptor. Also, the necessary relationship between the two was calculated and implemented in the computation part, which proves to be an advantage over some other pipelineable structures [4] in the sense that denormalized unit can be used in combination with an inverse pair of real multipliers. The importance of this is significant when the ripple frequency responses were compared and the complex cross adaptor represented by a denormalized cross adaptor and two multipliers, gave a response that was much closer to the nominal value, hence being less sensitive. In addition, calculations for the time domain were implemented on the PU blocks used for the digital domain calculations and the output results were more than satisfactory, being very close to the nominal value and to their digital domain counterparts.

The time domain calculations were useful in providing a more descriptive way of presenting the computational steps used in the basic PU building blocks with complex cross adaptors and pairs of inverse real multipliers. These are advantages that can be applied in the field of VLSI implementation because of the lower number of independent coefficients, which decreases computational and design overhead. The results were calculated using quantized coefficients with different precision producing satisfactory results as mentioned above. The other advantage is that this structure does not require outside complex multipliers to preserve planar rotation, because everything is done internally inside of the two-port adaptor. Also, the way these formula and computation steps were implemented provides an easy way of creating a filter of any order. A very important feature to notice is that this entire work is done using fully pipelineable structures, hence further increasing the computational speed of the actual filter and the design process. Pipelineability provides for the operations of the processor to be fragmented into sequential tasks that are performed in parallel. This can be seen from the time-domain realization where delays are being used for the next computational step before present one has completed. The slowest task is the one that determines the computational speed in this case and the overall delay of the procedure is the sum of the all delays related to the individual tasks. This parallelism enables the accumulation and retrieving of the next instruction at the same time. Many research articles actually deal with the design and the theoretical approach to pipelineable structures [17], [18], [19] so we will not address this topic any further in this concluding chapter. New content and the advantage of the approach derived in this thesis can be seen in the DSP implementation that each step has both the multiplication and the addition step in each of the computing cycles. Also, only one coefficient is used, hence making the implementation easier. The recommendations for future work could be in the sense of further exploration of the various two-port realizations of digital filters using PU building blocks to obtain those most suitable for VLSI designs or further work on the topic of the cross adaptors used as building blocks with increased computation speed and easier implementation.

REFERENCES

[1] S. K. Rao and T. Kailath, "Orthogonal Digital Filters for VLSI Implementation", IEEE Trans. Circuits Syst., vol. CAS-31, no. 11, pp. 933-945, Nov. 1984.

[2] A. Fettweis, "Wave Digital Filters: Theory and Practice", Proc. IEEE, vol. 74, pp. 270-327, Feb. 1986.

[3] V. Belevitch, "Classical Network Theory", San Francisco, CA: Holden-Day, 1986.

[4] V. Cheng, "Synthesis of Modular and Pipelineable Wave Digital Filters", M. Sc. Thesis, University of Manitoba, Winnipeg, Canada, 1992.

[5] J. Wang, "Design of Even-Order Complex Wave Digital Filters", M. Sc. Thesis, University of Manitoba, Winnipeg, Canada, 1996.

[6] A. Fettweis, "Scattering Properties of Real and Complex Lossless 2-Ports", IEEE vol. 128, Pt. G, No. 4, Aug. 1981.

[7] M. R. Jarmasz, "A Simplified Synthesis of Lossless Two-Port Wave Digital and Analog Filters", Ph.D. Thesis, University of Manitoba, Winnipeg, Canada, 1990.

[8] K. A. Owenier, "Optimization of Wave Digital Filters with Reduced Number of Multipliers", AEÜ, Band 30, pp. 387-393, 1976.

[9] M. R. Jarmasz, V. Cheng and G. O. Martens, "Synthesis of Pipelineable Complex Wave Digital Filters", IEEE, vol. 41, No. 2, Feb. 1994.

[10] A. Fettweis, "Passivity and Losslessness in Digital Filters", AEÜ, vol. 42, No. 1, pp. 1-8, Jan/Feb. 1988.

[11] A. Fettweis, "Pseudopassivity, Sensitivity and Stability of Wave Digital Filters", IEEE Trans. Circuit Theory, vol. CT-19, pp. 668-673, Nov. 1972.

[12] G. Scarth, Notes, University of Manitoba, Winnipeg, Canada, Sep./Dec. 1996.

[13] A. Antoniou, "Digital Filters", Highstown, McGraw-Hill, 1993.

[14] G. Scarth, "Cascade Realization of Complex Wave Digital and Analog Networks", Ph. D. Thesis, University of Manitoba, Winnipeg, Canada, Feb. 1992.

[15] G. Scarth and G. O. Martens, "Synthesis of Complex Lossless Two-Ports", Int. J. Circuit Theory Appl., vol. 22, pp. 121-143, 1994.

[16] A. Fettweis, "Principles of Complex Wave Digital Filters", Int. J. Circuit Theory Appl., vol. 9, pp. 119-134, Apr. 1981.

[17] J. JaJa and A. Kapoor, "Parallel and Pipelined VLSI Architectures Based on Decomposition", IEEE Press Books, 1986.

[18] Don Morgan, "Practical DSP Modeling, Techniques and Programming in C", New York, John Wiley & Sons, 1994.

[19] S. Y. Kung, "VLSI and Modern Signal Processing", New Jersey, Prentice-Hall 1985.

[20] H. Schütte, "On Adaptors for Complex Wave Digital Filters", Proc. IEEE Int. Symp. On Circuits and Systems, Portland, OR, May 1989, Vol. 3, IEEE, New York, 1989, pp. 1644-1647.

[21] K. Meerkötter, "Complex Passive Networks and Wave Digital Filters, " Proc. Eur. Conf. on Circuit Theory and Design (Warsaw, Poland, Sept. 1980), vol.2, pp.24-235.

[22] G. O. Martens, notes on Mapping from the Ψ-domain to the z-domain, Jan. 1998, Winnipeg.

[23] A. Fettweis, "Modified Wave Digital Filters for Improved Implementation by Commercial Digital Signal Processors", Signal Processing, 16, 1989, P.193-207, Germany.

APPENDIX

Mapping from the Ψ-domain to the z-domain

The scattering matrix (in the ψ-domain) for lossless two ports has the representation

$$S = \frac{1}{g(\psi)} \cdot \begin{pmatrix} h(\psi) & \sigma \cdot f(\psi) \\ f(\psi) & -\sigma \cdot h(\psi) \end{pmatrix} \qquad \text{(A.1a)}$$

where σ is a unimodular constant ($|\sigma|=1$), f, g, and h are polynomials and g is a Hurwitz polynomial.

$f_*(\psi)=f^*(-\psi^*)$, similarly for h_*, and f, g and h satisfy

$$gg_*=hh_*+ff_* \qquad \text{(A.1b)}$$

From the above equation it follows that n=deg g, l=deg h, m=deg f satisfy $l, m \le n$.

The polynomials can be represented in the form

$$g(\psi) = \sum_{i=0}^{n} g_i \cdot \psi^i \quad , \quad f(\psi) = \sum_{i=0}^{m} f_i \cdot \psi^i \quad , \quad h(\psi) = \sum_{i=0}^{l} h_i \cdot \psi^i \qquad \text{(A.2)}$$

where g_i, f_i and h_i are constants.

Define $\tilde{g}(z) = (z+1)^n \cdot g(\psi)$ with $\psi = \frac{z-1}{z+1}$

$$= (z+1)^n \cdot \sum_{i=0}^{n} g_i \cdot \left(\frac{z-1}{z+1}\right)^i$$

$$= \sum_{i=0}^{n} \tilde{g}_i \cdot z^i \qquad \text{where the } \tilde{g}_i \text{ are new constants.} \qquad \text{(A.3a)}$$

Similarly,

$$\tilde{f}(z) = (z+1)^{n-m} \cdot \sum_{i=0}^{m} \tilde{f}_i \cdot z^i \qquad \text{(A.3b)}$$

Thus $\frac{f(\psi)}{g(\psi)}$ maps to $\frac{\tilde{f}(z)}{\tilde{g}(z)}$

by definition $f_*(\psi) = f^*(-\psi^*)$

$$= \sum_{i=0}^{m} f_i(-\psi)^i = \sum_{i=0}^{m} f_i(-1)^i\psi^i \qquad \text{(A.4)}$$

Consider the mapping of $f_*(\psi)$:

$$(z+1)^n f_*(\psi) = (z+1)^n \sum_{i=0}^{m} f_i(-1)^i \left(\frac{z-1}{z+1}\right)^i \qquad \text{(A.5)}$$

Also,

$$\tilde{f}_*(z) = z^n \cdot \tilde{f}^*\left(\frac{1}{z^*}\right)$$

$$= (z+1)^n \sum_{i=0}^{m} f_i(-1)^i \left(\frac{z-1}{z+1}\right)^i \qquad \text{(A.6)}$$

Obviously Eq. A.5 is equvalent to Eq. A.6.

The same approach is used for $h_*(\psi)$ and $\tilde{h}_*(z)$.

Therefore

$$S = \frac{1}{\tilde{g}(z)} \cdot \begin{pmatrix} \tilde{h}(z) & \sigma\cdot\tilde{f}(z) \\ \tilde{f}(z) & -\sigma\tilde{h}_*(z) \end{pmatrix} \qquad \text{(A.7)}$$

All the zeros of $\tilde{g}(z)$ are inside the unit circle in the z-plane and clearly Eq. A.1b is satisfied.

To express the polynomials in terms of z^{-1}, multiply the numerators and the denominator in S by z^{-n} (n = deg $\tilde{g}(z)$).

Denote the polynomials in z^{-1} by a "hat".

Then

$$\hat{f}_*(z^{-1}) = z^{-n}\,\hat{f}^*(z^*) \tag{A.8}$$

and

$$S = \frac{1}{\hat{g}(z^{-1})}\begin{pmatrix} \hat{h}(z^{-1}) & \sigma\cdot\hat{f}_*(z^{-1}) \\ \hat{f}(z^{-1}) & -\sigma\cdot\hat{h}_*(z^{-1}) \end{pmatrix} \tag{A.9}$$

IMAGE EVALUATION
TEST TARGET (QA-3)

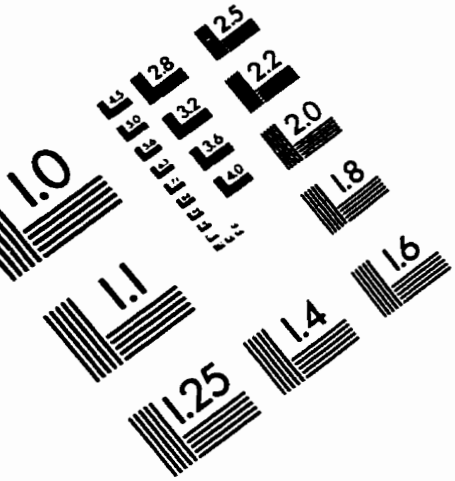

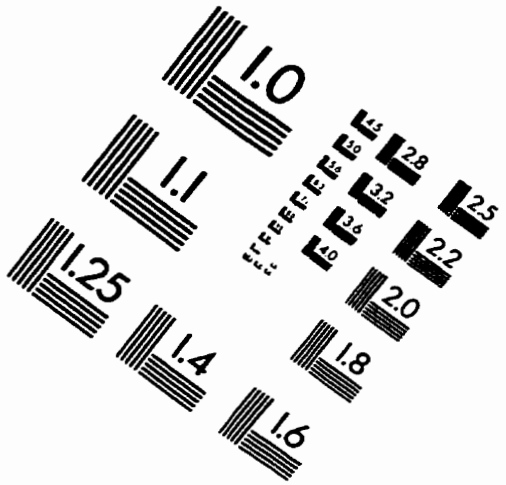

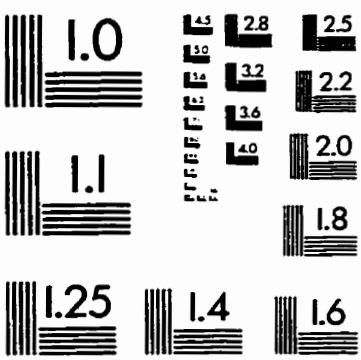

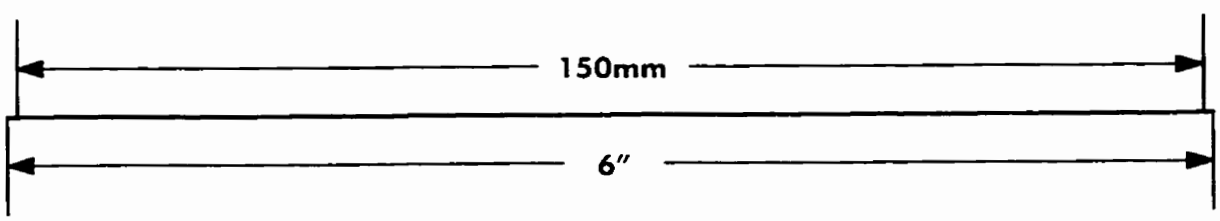

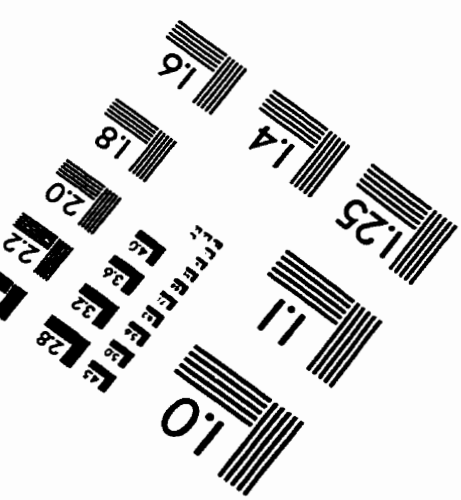

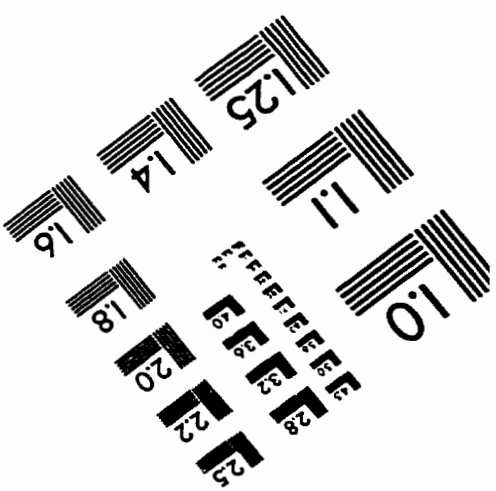

APPLIED IMAGE, Inc
1653 East Main Street
Rochester, NY 14609 USA
Phone: 716/482-0300
Fax: 716/288-5989